RESEARCH ARTICLE

Exosomes mediate LTB$_4$ release during neutrophil chemotaxis

Ritankar Majumdar[1], Aidin Tavakoli Tameh[1], Subhash B. Arya[2,3], Carole A. Parent[1,2,3,4,5]*

1 Laboratory of Cellular and Molecular Biology Center for Cancer Research, NCI, NIH, Bethesda, Maryland, United States of America, **2** Department of Pharmacology, University of Michigan Medical School, Ann Arbor, United States of America, **3** Life Sciences Institute, University of Michigan, Ann Arbor, Michigan, United States of America, **4** Department of Cell and Developmental Biology, University of Michigan Medical School, Ann Arbor, Michigan, United States of America, **5** Rogel Cancer Center, University of Michigan Medical School, Ann Arbor, Michigan, United States of America

* parentc@umich.edu

Abstract

Leukotriene B$_4$ (LTB$_4$) is secreted by chemotactic neutrophils, forming a secondary gradient that amplifies the reach of primary chemoattractants. This strategy increases the recruitment range for neutrophils and is important during inflammation. Here, we show that LTB$_4$ and its synthesizing enzymes localize to intracellular multivesicular bodies, which, upon stimulation, release their content as exosomes. Purified exosomes can activate resting neutrophils and elicit chemotactic activity in an LTB$_4$ receptor-dependent manner. Inhibition of exosome release leads to loss of directional motility with concomitant loss of LTB$_4$ release. Our findings establish that the exosomal pool of LTB$_4$ acts in an autocrine fashion to sensitize neutrophils towards the primary chemoattractant, and in a paracrine fashion to mediate the recruitment of neighboring neutrophils in trans. We envision that this mechanism is used by other signals to foster communication between cells in harsh extracellular environments.

Author's note

Concerns have emerged about the immunoelectron microscopy results originally reported in the article by Majumdar and colleagues [1]. In addition, errors were made in the scale bars reported in Figs 2H and 3D of the same article. Accordingly, this article has been retracted. We are grateful for the opportunity to republish a version of this article in which the electron microscopy data have been removed. None of the major conclusions attained in the original article are affected by the removal of the contentious data. We sincerely apologize to *PLOS Biology* and the scientific community at large for this occurrence.

Introduction

Chemotaxis, the directed movement of cells in response to external chemical gradients, is essential to a wide array of biological processes ranging from developmental processes, wound

Abbreviations: AA, arachidonic acid; cAMP, cyclic adenosine monophosphate; CD63-GFP, GFP-tagged CD63; CI, chemotaxis index; CsH, cyclosporin H; ER, endoplasmic reticulum; FLAP, 5-LO activating protein; fMLP, N-formylMethionyl-Leucyl-Phenylalanine; GM–CSF, granulocyte macrophage–colony-stimulating factor; KD, knockdown; KO, knockout; LTA$_4$, leukotriene A$_4$; LTA$_4$H, LTA$_4$ hydrolase; LTB$_4$, leukotriene B$_4$; LTB$_4$R1, receptor for LTB$_4$; mCherry-5LO, mCherry-tagged 5-LO; MLCII, myosin light chain II; MMP9, matrix metallopeptidase 9; MPO, myleoperoxidase; MVB, multivesicular body; NSshRNA, nonspecific shRNA; shRNA, small hairpin RNA; 5-LO, 5-lipoxygenase.

healing, angiogenesis, and immune responses and is implicated in pathological conditions such as chronic inflammatory diseases and metastasis [2]. Upon exposure to endpoint primary chemoattractants, cells secrete secondary chemoattractants that serve to maintain the robustness and sensitivity to the primary chemoattractant signals [3]. Once secreted, these secondary chemoattractants form a gradient to recruit cells that are farther away, thereby dramatically increasing the range and persistence of detection [4]. Intercellular communication through the release of secondary chemoattractants may be homotypic, where the primary and secondary chemoattractant are the same, or it may be heterotypic, where the secondary chemoattractant is different from the primary chemoattractant and is released following stimulation by primary attractants. Homotypic intercellular communication is remarkably exhibited in the social amoebae *Dictyostelium discoideum*, where collective chemotaxis of cells towards cyclic adenosine monophosphate (cAMP) is regulated by the release of cAMP and the formation of characteristic chains of cells called streams [5]. Unlike cAMP in *Dictyostelium*, the release of the secondary chemoattractants CCL3 and CXCL8 by monocytes and dendritic cells in response to the primary chemoattractant Serum Amyloid A represents an example of heterotypic intercellular communication [6]. This ability of chemotaxing cells to transduce autocrine and paracrine chemical signals in response to primary signals has been termed signal relay.

Heterotypic signal relay occurs in neutrophils migrating towards primary chemoattractant gradients through the release of leukotriene B$_4$ (LTB$_4$) [7]. Following stimulation, cytoplasmic phospholipase A$_2$α translocates to the nuclear envelope, where it is poised to hydrolyze membrane bound lipids to form arachidonic acid (AA) [8]. Simultaneously, 5-lipoxygenase (5-LO) is mobilized to the nuclear envelope where it associates with the 5-LO activating protein (FLAP) and acts on AA to generate leukotriene A$_4$ (LTA$_4$). LTA$_4$, by means of LTA$_4$ hydrolase (LTA$_4$H), is finally converted into LTB$_4$ [8], which is then secreted from cells by an unknown mechanism. Initially thought to be released at the site of infection to mediate neutrophil recruitment and proinflammatory processes [9] [10], LTB$_4$ was later shown to be a central secondary chemoattractant in vivo [11]. More recently, we showed that LTB$_4$ preferentially mediates neutrophil swarming towards tissue injury sites [12] and established that the secreted LTB$_4$ in physiological gradients of primary chemoattractants acts as an amplifier of neutrophil chemotaxis and mediates signal relay between migrating neutrophils [7].

In order for secondary chemoattractants to act as bona fide signal relay molecules, they must be released in a form that enables the generation of stable gradients during chemotaxis. It has been established that the release and subsequent diffusion of LTB$_4$ creates extremely transient gradients due to the small size of the molecule [13]. The self-diffusion coefficient of a typical formyl chemoattractant is approximately 10^{-5} cm^2/s, which is a log order of magnitude higher than typical unsaturated fatty acids [14]. This implies extremely shallow LTB$_4$ concentration profiles. Indeed, assessment of the diffusive properties of AA, the structurally similar precursor of LTB$_4$, shows shallow and transient gradients compared to a primary chemoattractant such as N-formylMethionyl-Leucyl-Phenylalanine (fMLP) [13]. As a plausible mechanism to generate stable secondary gradients, one may argue in favor of a carrier-based mechanism for passive LTB$_4$ transport, such as binding to serum albumin, and this may indeed be true for systemic transport [15]. This, however, would not account for short-range gradients in migrating cells owing to protracted and uncontrolled LTB$_4$ release. Moreover, this mechanism would not explain how hydrophobic molecules such as LTB$_4$ are protected from the aqueous environment of the extracellular milieu.

The mechanisms by which LTB$_4$ is secreted and how LTB$_4$ gradients are formed or mediate signal relay of primary chemotactic signals have yet to be determined. However, studies on gradient formation of lipid-modified *Drosophila* morphogens [16], or the formation of palmitoylated-Wnt gradients during *Drosophila* embryogenesis [17] and cAMP gradient propagation in *Dictyostelium* [18], point towards vesicular packaging as an effective way of signal
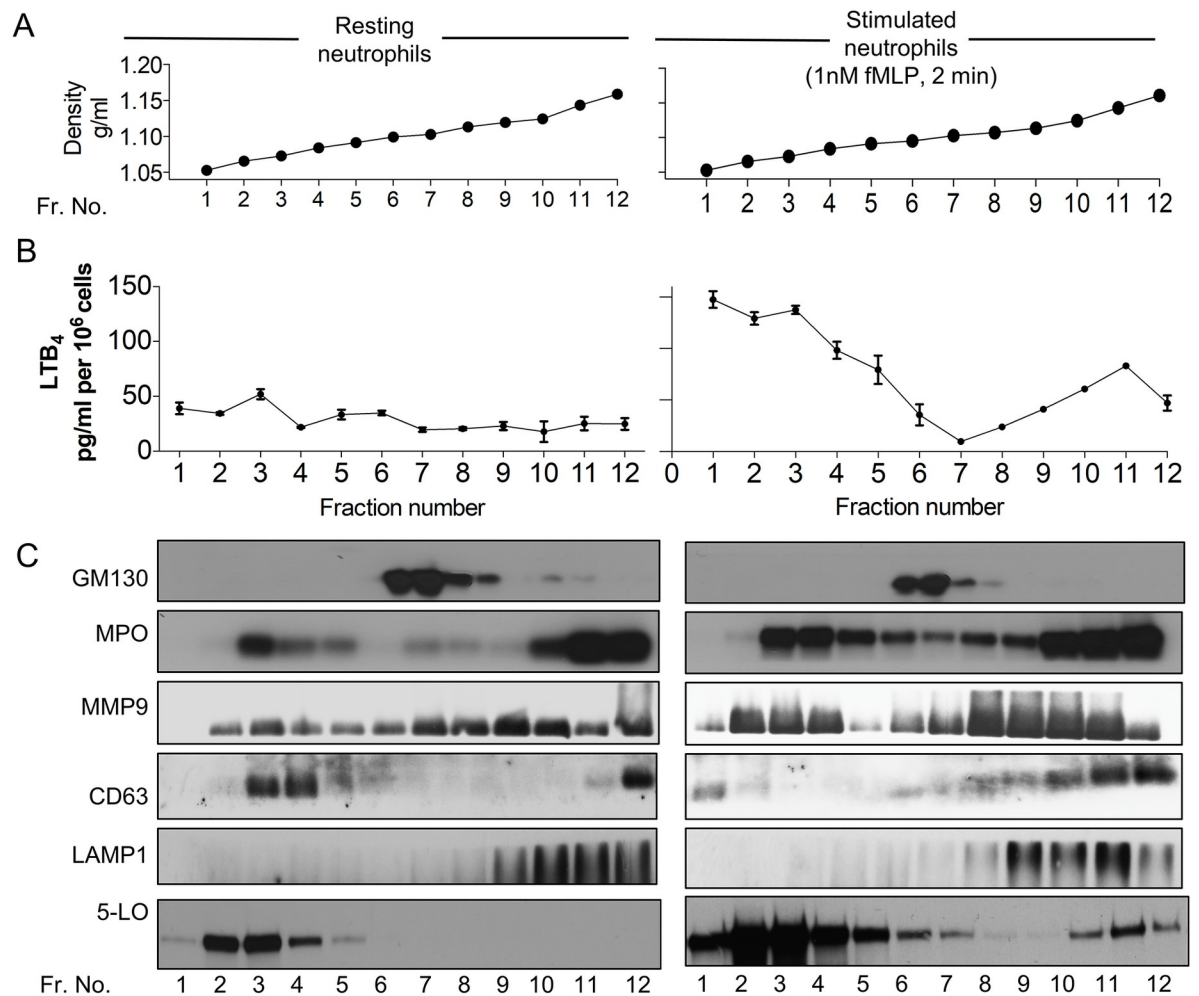
Fig 1. LTB$_4$ and 5-LO partition with CD63 and LAMP1 positive fractions in continuous iodixanol gradients. (**A**) Mock-loaded continuous iodixanol gradients were fractionated and the density of each fraction determined as described. (**B**) Nitrogen cavitates of freshly isolated primary human neutrophils were density fractionated on iodixanol gradients, and LTB$_4$ content from each fraction was extracted and measured by EIA. (**C**) Total protein from each fraction of iodixanol gradient described in panel B was TCA precipitated, and western analysis was performed using specific antibodies. Data are representative of 2–6 independent experiments. Raw data for panels A and B can be found in the Supporting information section S1 Data file, and uncropped blots for panel C can be found in the S1 Raw images file. fMLP, N-formylMethionyl-Leucyl-Phenylalanine; LTB$_4$, Leukotriene B$_4$; MMP9, matrix metallopeptidase 9; MPO, myleoperoxidase; TCA, trichloroacetic acid; 5-LO, 5-lipoxygenase.

https://doi.org/10.1371/journal.pbio.3001271.g001

dissemination in the extracellular milieu. In the present study, we investigated whether a similar vesicular packaging of LTB$_4$ is involved in the creation of a stable gradient during neutrophil chemotaxis. To do so, we assessed whether LTB$_4$ is secreted though extracellular vesicles and if its synthesis and transport involve intracellular vesicular trafficking. Most importantly, we also determined if vesicles released during chemotaxis are indeed capable of mediating the LTB$_4$-dependent signal relay response during neutrophil chemotaxis.

Results

### 5-LO translocates to CD63 and LAMP1 positive fractions upon fMLP addition

To begin identifying the mechanisms that underlie LTB$_4$ secretion, we measured LTB$_4$ content as well as the distribution of 5-LO in resting and activated neutrophils. We fractionated

unstimulated and fMLP-stimulated primary human neutrophils using nitrogen cavitation, differential centrifugation, and separation on iodixanol density gradients (Fig 1A). In resting neutrophils, LTB$_4$ content was primarily low across the different fractions with a small peak observed in fraction 3 (Fig 1B). On the other hand, in fMLP-stimulated neutrophils, a nonuniform asymmetric increase of LTB$_4$ levels was observed, where LTB$_4$ levels were elevated in both low- (fractions 1 to 5; density approximately 1.05 to 1.08 g/ml) and high-density fractions (fractions 10 to 12; density approximately 1.17 to 1.19 g/ml), but not in intermediate density fractions (fractions 6 to 9; approximately 1.09 to 1.11 g/ml) that contained the *cis*-Golgi markers GM130 (Fig 1B and 1C). This fMLP-induced asymmetric partitioning of LTB$_4$ across different densities was unlike other canonical secretory proteins such as myleoperoxidase (MPO —a marker for the azurophilic granules) and matrix metallopeptidase 9 (MMP9—a marker for gelatinase granules) [19], although total MPO and MMP9 levels appeared to increase poststimulation (Fig 1C). These findings suggest that canonical secretory pathways used by MMP9 and MPO are not involved in LTB$_4$ trafficking. On the other hand, fMLP stimulation did induce the redistribution of the tetraspannin CD63 to higher density fractions. As CD63 is known to traffic between late endosomal and secretory compartments such as multivesicular bodies (MVBs) [20], we reasoned that CD63 redistributes to MVBs upon fMLP addition. This was confirmed by the presence of LAMP1, a high-density lysosomal marker shown to be present in MVBs of neutrophils [21], in fractions 9 to 12 (Fig 1C). Remarkably, 5-LO was also found in CD63- and LAMP1-positive high-density fractions upon fMLP stimulation, and the distribution pattern of LTB$_4$ was similar to that of 5-LO in both resting and activated conditions, suggesting active 5-LO in this cellular compartment. Together, the presence of LTB$_4$ and 5-LO in CD63- and LAMP1-positive fractions suggest the involvement of MVBs in LTB$_4$/5-LO transport.

Neutrophils release exosomes containing LTB$_4$ and LTB$_4$ synthesizing enzymes upon fMLP addition

We next assessed the cellular distribution of 5-LO and CD63 in live chemotaxing cells. We expressed mCherry-tagged 5-LO (mCherry-5LO) and/or GFP-tagged CD63 (CD63-GFP) in the pluripotent hematopoietic cell line PLB-985, which can be differentiated into neutrophil-like cells [22]. We found that 5-LO localizes to the nucleus in resting mCherry-5LO cells (S1A Fig, S1 Movie). However, upon uniform fMLP addition, we readily observed the redistribution of mCherry-5LO to the cytoplasm in a punctate pattern (Fig 2A, S2 Movie). This vesicular localization was even more apparent in cells chemotaxing in a gradient of fMLP and was found to be more prominent at the trailing edge compared to the leading edge of chemotaxing cells (Fig 2B, S3 Movie). The trailing edge localization of 5-LO containing vesicles was further substantiated through phalloidin counterstaining, which marks the leading edge F-actin (S1B Fig). To determine the nature of the 5-LO positive vesicles, we visualized the dynamic distribution of CD63-GFP. As expected, we observed a punctate localization of the MVB marker in both resting (S1A Fig) and stimulated (S1C Fig) cells expressing CD63-GFP. Remarkably, in mCherry-5LO/CD63-GFP co-expressing cells chemotaxing towards fMLP, we observed a clear co-localization of both proteins (Fig 2C, S4 Movie), which again occurred mainly at the trailing edge of the chemotaxing cells.

As we observed co-localization of mCherry-5LO with CD63-GFP, we next set out to determine whether neutrophils secrete exosomes that contain LTB$_4$ and LTB$_4$ synthesizing enzymes. Supernatants from fMLP-stimulated neutrophils fractionated on a discontinuous gradient of iodixanol yielded a uniform vesicle population with an average inner diameter size of 36.4 nm as measured from electron microscopy images (Fig 2D). The hydrodynamic
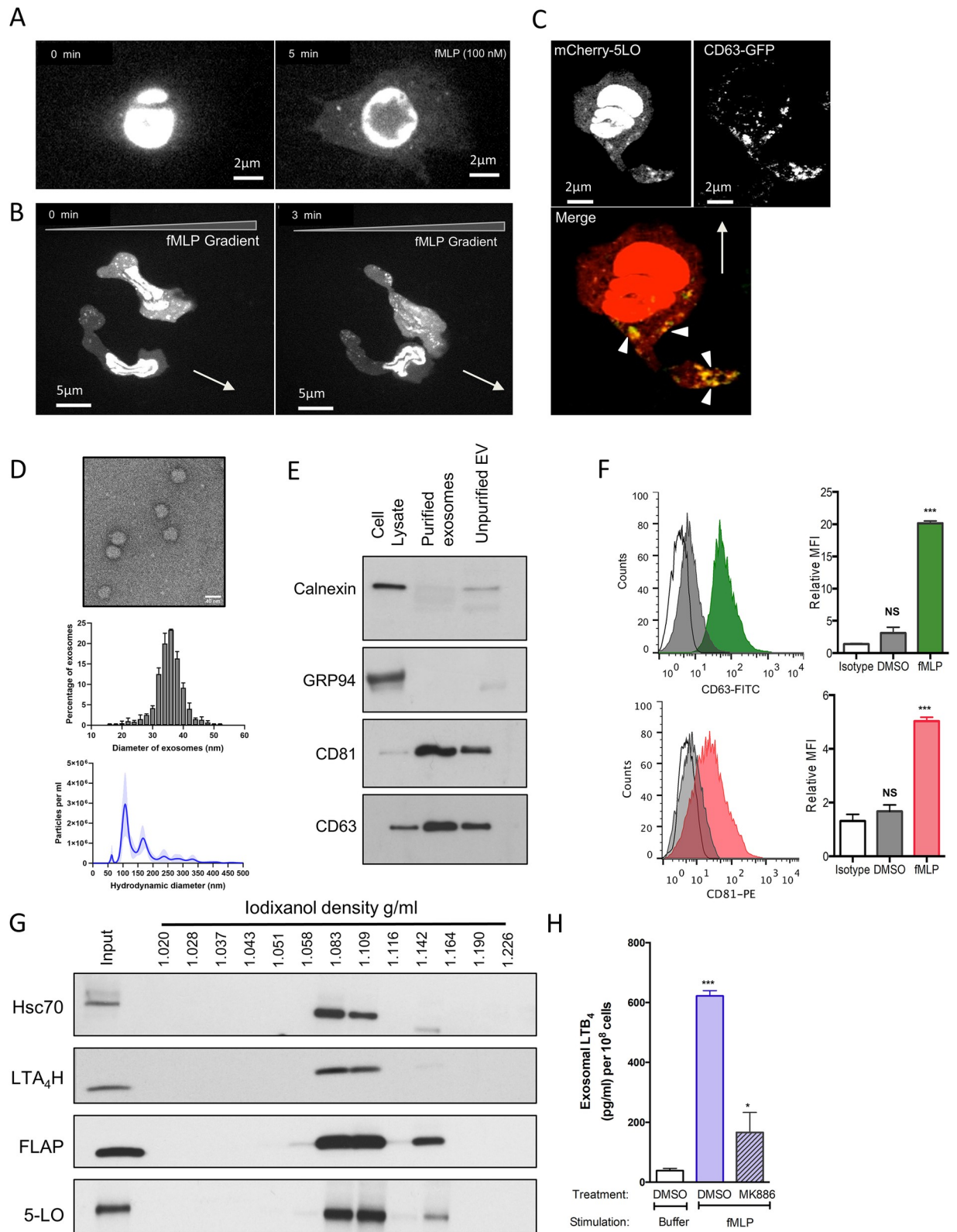
Fig 2. Neutrophils release exosomes containing LTB$_4$ and LTB$_4$ synthesizing enzymes upon fMLP addition. (A) Differentiated mCherry-5LO cells were plated on fibronectin-coated plates and time-lapse images were captured before and after a uniform stimulation with 10 nM fMLP. Fluorescent images are representative of 6 independent experiments. Also see S1 and S2 Movies. **(B)** Differentiated mCherry-5LO cells

were allowed to chemotax under agarose towards an fMLP gradient. Time-lapse images were captured 30 min after the addition of fMLP, 700 μm away from the chemoattractant well. Gradient slope approximately 50 pM/μm (see Materials and methods). Fluorescent images are representative of 20 independent experiments. Also see S3 Movie. **(C)** Differentiated CD63-GFP/mCherry-5LO co-expressing cells were allowed to chemotax as described in B. Fluorescent images are representative of 8 independent experiments. Also see S1 Fig and S4 Movie. **(D)** Upper panel: Representative negatively stained EM image of vesicles after purification on a discontinuous iodixanol gradient. Middle panel: Plot depicting the vesicle sizes determined from 600 vesicles from 3 independent experiments (plotted as mean +/− SEM). Bottom panel: Representative nanoparticle tracking analysis of 3 independent experiments (plotted as mean +/− SEM of 5 technical replicates). **(E)** Equal amounts of protein from purified exosomes, crude ultracentrifugation pellets, and total cell lysates (10 μg) were subjected to western analysis using Calnexin, GRP94, CD81, and CD63 specific antibodies. Results are representative of 3 independent experiments. **(F)** Detection of CD63 (upper panel) or CD81 (lower panel) on exosomes obtained from fMLP-stimulated or DMSO-treated neutrophils in a bead-based flow cytometry assay. Relative median fluorescence intensities obtained from 3 independent experiments are shown as mean ± SD. *** and NS indicate $p < 0.0001$ and $p > 0.05$, respectively, compared to the isotype control. Also see S2 Fig. **(G)** Crude ultracentrifugation pellets were loaded on a discontinuous iodixanol gradient, total protein from each fraction precipitated and subjected to western analysis using antibodies for the exosomal marker HSC70 or LTB$_4$ synthesizing enzymes. Approximately 5% of the total input was analyzed. Results are representative of 3 independent experiments. **(H)** Purified exosomes from fMLP-stimulated neutrophils treated with DMSO or MK886 (1 μM, 30 min) were lysed and their LTB$_4$ content measured using EIA. Results from 4 independent experiments are shown as mean ± SD. *** and NS indicate $p < 0.0001$ and $p > 0.05$, respectively, compared to the LTB$_4$ content of exosomes purified from vehicle treated nonstimulated cells. Raw data for panels F and H can be found in the Supporting information section S1 Data file. Uncropped blots for panels E and G can be found in the S1 Raw images file. CD63-GFP, GFP-tagged CD63; EM, electron microscopy; EV, extracellular vesicle; FLAP, 5-LO activating protein; fMLP, N-formylMethionyl-Leucyl-Phenylalanine; LTA$_4$H, LTA$_4$ hydrolase; LTB$_4$, leukotriene B$_4$; mCherry-5LO, mCherry-tagged 5-LO; MFI, mean fluorescence intensity; NS, not significant; 5-LO, 5-lipoxygenase.

https://doi.org/10.1371/journal.pbio.3001271.g002

diameter, determined using nanoparticle tracking analysis, gave rise to a major peak diameter of 108 nm (Fig 2D)—a characteristic size for exosomes [23]. The difference observed in particle size between these 2 methods is likely related to the dehydration that takes place when preparing membrane-bound vesicles for negative staining and electron microscopy. We found that the purified vesicles were enriched in the tetraspannins CD63 and CD81, also reported in exosomes [24], and had very low amounts of the endoplasmic reticulum (ER) integral protein Calnexin or the ER lumen marker GRP94 (Fig 2E). Furthermore, the possibility of contamination from ectosomes and other plasma membrane-derived vesicles was excluded by the absence of the ectosome marker CD11b in purified vesicles [25] (S2A Fig). We also found that the release of exosomes from neutrophils increased upon fMLP addition, as the detection of the exosomal markers CD63 and CD81 increased with fMLP treatment (Fig 2F). This increase was dependent on the concentration of fMLP added to cells (S2B Fig). Moreover, the release of exosomes from cells was also observed following ionomycin addition but not with granulocyte macrophage–colony-stimulating factor (GM–CSF) treatment (S2C and S2D Fig). Most importantly, we determined that the enzymes responsible for the synthesis of LTB$_4$, namely 5-LO, FLAP, and LTA$_4$H, were all present in fractions containing HSC70 (another known exosome marker [26]) (Fig 2G). The exosomes isolated from fMLP-stimulated neutrophils showed a high LTB$_4$ content, which was dramatically reduced by pretreating neutrophils with the FLAP inhibitor MK886 (Fig 2H). Together, these findings show that upon fMLP addition, neutrophils release exosomes containing LTB$_4$ and the enzymes required for its synthesis.

Exosomes activate neutrophils in an LTB$_4$-dependent manner

We next studied the extent by which exosomes mediate the effects of LTB$_4$ on neutrophil function. We first purified exosomes from mCherry-5LO and CD63-GFP expressing cells following fMLP treatment in the presence and absence of MK886 and measured their LTB$_4$ content. We found that the exogenous expression of either mCherry-5LO or CD63-GFP increases exosomal LTB$_4$ (Fig 3A) and, as we observed with neutrophils (Fig 2H), LTB$_4$ content was inhibited by pretreatment with MK886 (Fig 3A). Quantification of the released exosomes showed that the decrease in LTB$_4$ content in MK886-treated cells was not a result of a decrease in exosome release by these cells (Fig 3B). More importantly, the addition of exosomes derived from mCherry-5LO or CD63-GFP expressing cells to neutrophils rapidly induced cellular
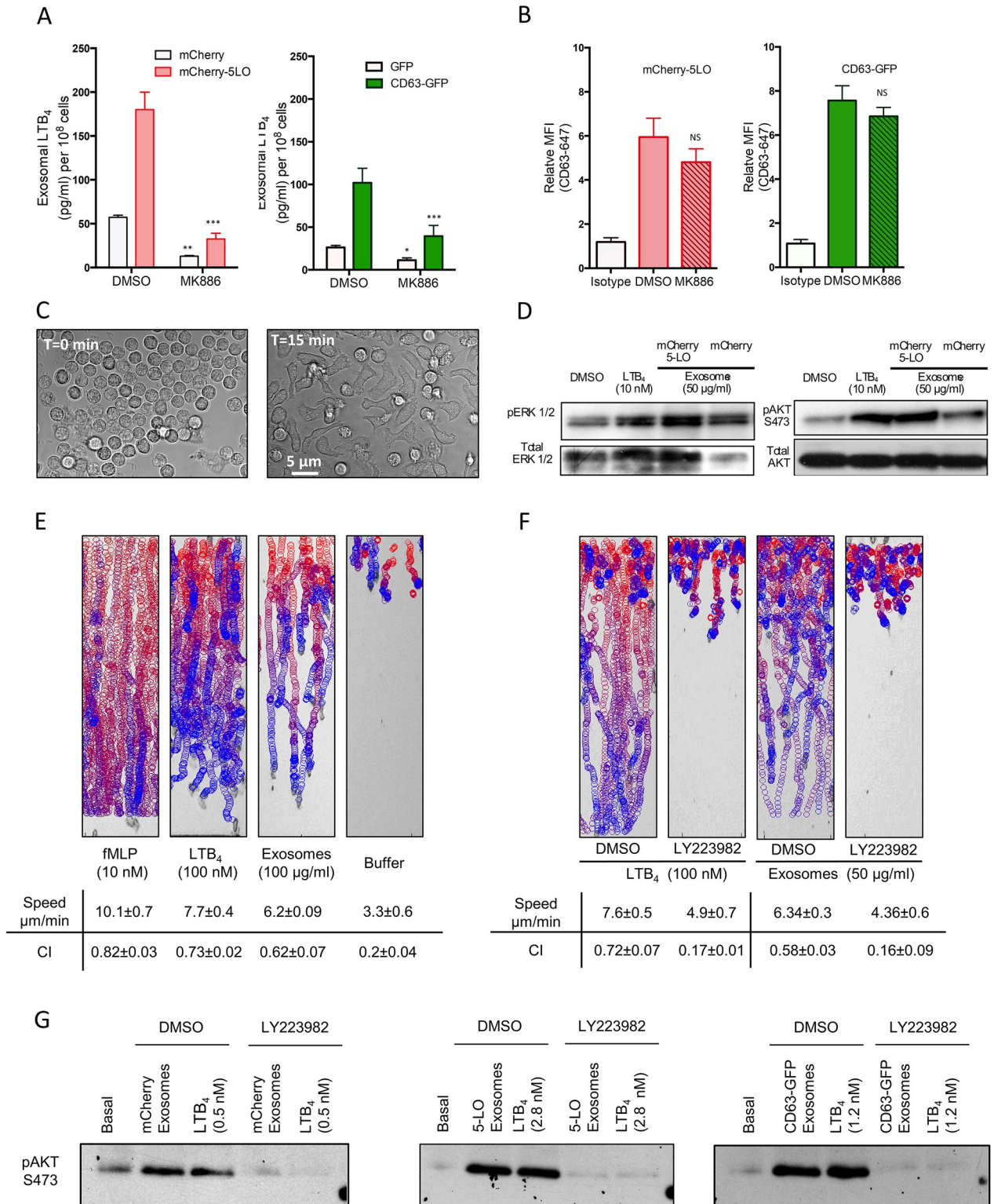
Fig 3. Exosomes activate neutrophils in an LTB$_4$-dependent manner. (A) Exosomes were purified from differentiated mCherry-5LO or CD63-GFP cells pretreated with either DMSO or MK886 (1 μM, 30 min) and subsequently stimulated with 2 nM fMLP. The exosomes were lysed and their LTB$_4$ content measured by EIA. Results from 4 independent experiments are shown as mean ± SD. The symbols ***, **, *, and NS indicate $p < 0.0001$, $p < 0.001$, $p < 0.01$, and $p > 0.05$, respectively, compared to corresponding DMSO-treated controls. **(B)** Detection of CD63 on exosomes purified from differentiated mCherry-5LO or CD63-GFP cells that were pretreated with either DMSO or MK886 (1 μM, 30 min) and subsequently

stimulated with 2 nM fMLP in a bead-based flow cytometry assay. Relative median fluorescence intensities obtained from 4 independent experiments are shown as mean ± SD. NS indicates statistical insignificance ($p > 0.05$) of the number of exosomes derived from MK886-treated cells compared to DMSO controls. **(C)** Neutrophil adhesion to fibronectin-coated plates was observed before and 15 min after the addition of 10 µg exosomes derived from CD63-GFP cells. Differential interference contrast images are representative of 3 independent experiments. **(D)** LTB$_4$ (10 nM) or exosomes (50 µg/ml) isolated from mCherry or mCherry-5LO cells was added to neutrophils for 15 min, and pAkt S473 and p44/42 MAPK (Erk1/2) (T202/Y204) were determined by western analysis using specific antibodies. Data are representative of 4 independent experiments. See S3A Fig for quantitation. **(E)** EZ-Taxiscan chemotaxis towards fMLP, LTB$_4$, exosomes derived from mCherry-5LO expressing cells, or control buffer. The images show paths of individual cells migrating as circles (from red to blue with increasing time) overlaid onto the final frame. Corresponding migration speeds and CI were calculated from 3 different experiments and represented as mean ± SD. Also see S5 Movie. **(F)** Neutrophils were treated with DMSO or LY223982 (10 µM for 30 min) and allowed to migrate towards LTB$_4$ or exosomes derived from mCherry-5LO expressing cells. Corresponding migration speeds and CI are calculated from 3 different experiments and represented as mean ± SD. Also see S3B Fig and S6 and S7 Movies. **(G)** Exosomes derived from mCherry, mCherry-5LO, or CD63-GFP expressing cells were divided into 2 parts. One part was used to measure LTB$_4$ levels to be added exogenously to neutrophils (control or LY223982 treated). The other part was added to neutrophils and pAkt (S473) levels were assessed after 15 min incubation. Data are representative of 3 independent experiments. See S3C Fig for quantification. Raw data for panels A and B can be found in the Supporting information section S1 Data file. Uncropped blots for panels D and G can be found in the S1 Raw images file. CD63-GFP, GFP-tagged CD63; CI, chemotaxis index; fMLP, N-formylMethionyl-Leucyl-Phenylalanine; LTB$_4$, leukotriene B$_4$; mCherry-5LO, mCherry-tagged 5-LO; MFI, mean fluorescence intensity; NS, not significant; 5-LO, 5-lipoxygenase.

polarization and adhesion, indicating that the exosomes readily activate resting neutrophils (Fig 3C). These observations were further strengthened by the increase of both pErk1/2 and pAkt levels upon the exogenous addition of exosomes from mCherry-5LO or mCherry expressing cells to resting neutrophils (Figs 3D and S3A). Of note, the extent by which the exosome preparations increased pErk1/2 and pAkt levels was greater in cells exposed to mCherry-5LO exosomes versus mCherry exosomes (S3A Fig), which could reflect the higher LTB$_4$ content of exosomes derived from mCherry-5LO expressing cells, compared to mCherry expressing cells (Fig 3A).

The EZ-Taxiscan microfluidic device was used to assess whether exosomes are capable of inducing a chemotactic response. As seen in Fig 3E and S5 Movie, neutrophils were able to migrate towards exosomes derived from mCherry-5LO expressing cells with speeds and chemotactic indices (CIs) comparable to those observed in the presence of LTB$_4$ alone. To determine whether the chemotactic response was mediated by LTB$_4$, we exposed neutrophils treated with the LTB$_4$ receptor-1 antagonist LY223982 to exosomes. We found that LY223982 treatment dramatically reduced the chemotactic response of neutrophils to both LTB$_4$ and exosomes derived from mCherry-5LO expressing cells (Fig 3F, S6 Movie). The antagonist-treated cells, however, did not show migration defects to saturating concentrations of fMLP, showing that LY223982 treatment did not impede chemotaxis due to nonspecific effects (S3B Fig). We also observed that exosomes derived from MK886-treated mCherry-5LO cells displayed weak chemotactic activity compared to exosomes from control treated cells (S7 Movie), further showing that the LTB$_4$ present in exosomes is responsible for the chemotactic behavior. These results were confirmed biochemically by assessing the effects of the exogenous addition of LTB$_4$ or exosomes on pAkt in neutrophils pretreated with LY223982. As shown in Fig 3G, LTB$_4$ or exosome addition gave rise to equal levels of pAkt for each exosome preparation and LTB$_4$ amounts used and, most importantly, the pAkt response was blocked by pretreating the cells with LY223982 (see S3C Fig, for quantification). Together, these findings establish the central role of LTB$_4$ in exosome-mediated neutrophil activation.

Reduced exosome production leads to a decrease in exosomal LTB$_4$ release and a loss in directional migration

To specifically assess the role of exosome formation and release for LTB$_4$ secretion, we knocked down Rab27a or neutral sphingomyelinase 1 (nSmase1; SMPD2 gene) using small hairpin RNAs (shRNAs) in PLB-985 cells. Rab27a is critical in MVB docking to the plasma membrane, and its depletion was shown to reduce exosome secretion [27,28]. nSmase is

important in exosome secretion by mediating the budding of exosomes into MVBs [29]. We achieved an efficient knockdown (KD) of Rab27a and nSmase1 expression in both undifferentiated and differentiated PLB-985, and the KD of one gene did not alter the expression of the other (S4A Fig). Of the 6 shRNA sequences screened for each gene, we selected Rab27a shRNA 1 (sh1) and Rab27a shRNA 3 (sh3) for further studies (presenting 75% ± 4% and 70% ± 8% reduction of protein levels, respectively), whereas shRNA 2 (sh2) and shRNA 4 (sh4) were selected for SMPD2 (presenting 82% ± 8% and 85% ± 6% reduction in protein levels, respectively). Using CD63 and CD81 as markers, we found that both SMPD2 and Rab27a KD cells show reduced exosome production upon treatment with 2 nM fMLP compared to control non-specific shRNA (NSshRNA) cells (Figs 4A and S4B). The purity of the exosome preparations was assessed using the ectosome marker CD11b. Similarly, LTB$_4$ content of purified exosomes from both KD cell lines was markedly lower than in control cell lines (Fig 4B), although LTB$_4$ levels across the different cell types were not different when normalized to the total exosomal protein content (Fig 4C). These findings indicate that depletion of either nSmase1 or Rab27a does not affect LTB$_4$ synthesis. When we measured the total amount of LTB$_4$ secreted from each cell line in response to 1 nM fMLP, a physiological relevant concentration, we also observed a 75% to 85% reduction in KD cells compared to control (Fig 4D). Interestingly, stimulating cells with a saturating concentration of fMLP (1 μM) reduced total LTB$_4$ secretion by 40% to 50%. Although this could result from residual Rab27a or nSmase1 activity in the KD cell lines, nonexosomal sources of LTB$_4$ could become dominant under bulk activation conditions.

We next set out to assess the chemotactic behavior of the KD cell lines. We found that KD of either SMPD2 or Rab27a specifically reduced the directional motility (or CI) of cells towards a subsaturating concentration of fMLP (effective concentration 1 nM) (Fig 4E and S8 Movie), as the speed of migration remained unchanged for both KD cell lines (Fig 4E). To further investigate whether exosomes play a role in the relay of primary chemotactic signals, we measured myosin light chain II (MLCII) phosphorylation following a subsaturating fMLP stimulation, a process acutely affected by the disruption of LTB$_4$ signaling in neutrophils [7]. As we previously reported, we measured an increase in pMLCII levels in cells expressing NSshRNA in response to 2 nM fMLP (Fig 4F). We also found that the increase of pMLCII levels was further accentuated in PLB-985 cells over expressing the receptor for LTB$_4$ (LTB$_4$R1), suggesting higher sensitivity of LTB$_4$R1 expressing cells towards signal relay processes and the pivotal role that LTB$_4$ plays in this response (Fig 4F). In sharp contrast, and as observed in neutrophils where LTB$_4$ synthesis is inhibited [7], no fMLP-mediated pMLCII increase was measured in either Rab27a or SMPD2 KD cells (Figs 4F and S4C). Together, these findings show that exosome release regulates LTB$_4$ secretion and signal relay during neutrophil chemotaxis.

Importantly, the defects of the KD cells appeared to be highly specific. Both SMPD2 and Rab27a KD cells did not show defects in their ability to adhere upon fMLP stimulation (S5A Fig), nor did they show any defect in their ability to increase pERK1/2 upon fMLP stimulation (S5B Fig). Furthermore, as we found with MK8886 treatment [7], the defects in directional migration were absent when a saturating concentration of fMLP (effective concentration 100 nM) was used (S5C Fig and S9 Movie). Together, these findings indicate that neither Rab27a nor nSmase1 regulate the ability of cells to respond to fMLP and rule out KD specific bystander effects.

Exosomal LTB$_4$ acts in an autocrine and paracrine fashion during neutrophil chemotaxis

We next sought to determine whether exosomal LTB$_4$ acts in an autocrine and/or paracrine fashion during neutrophil chemotaxis. To do so, we labeled neutrophils with cytotracker red
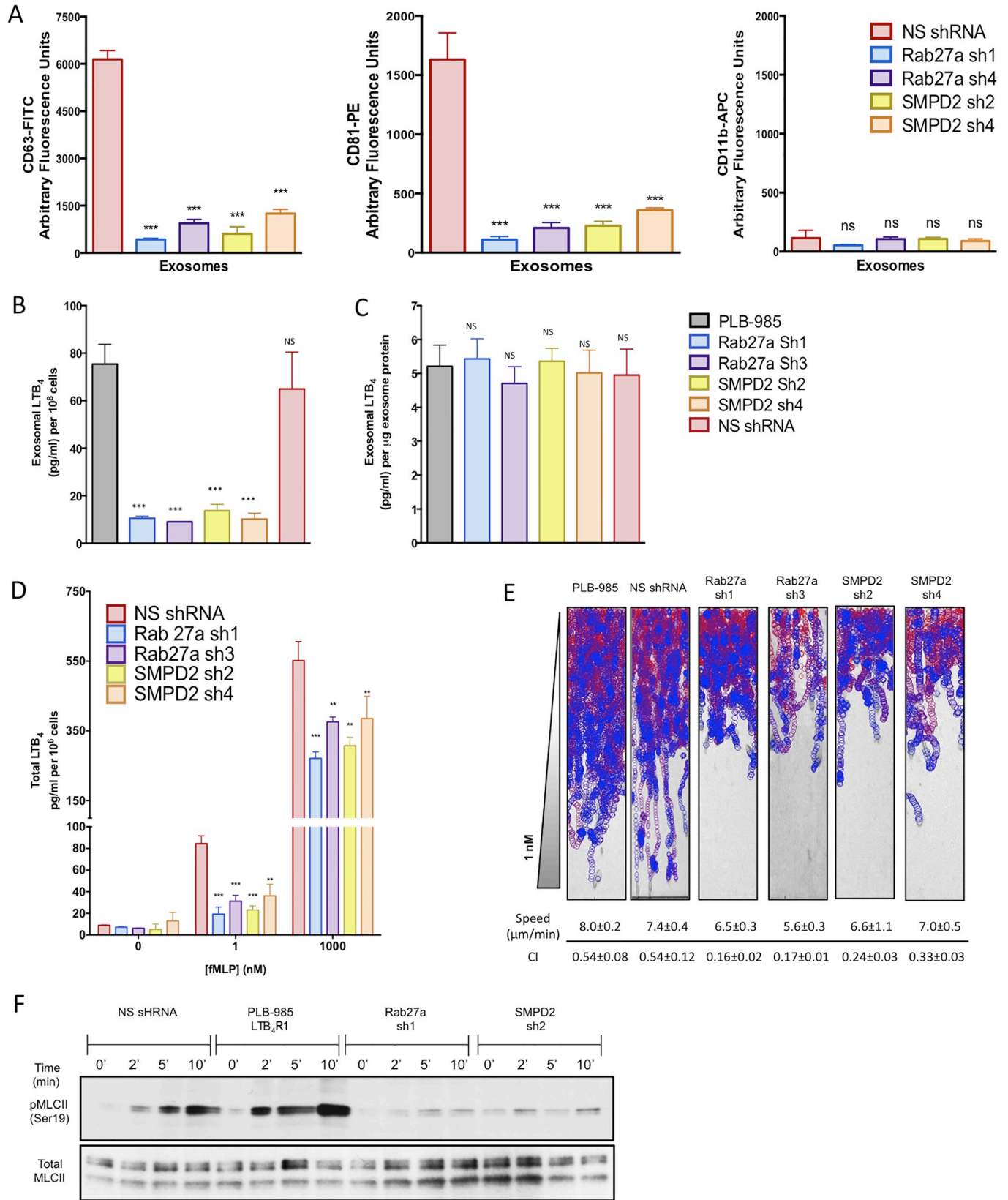
Fig 4. Rab27a and SMPD2 KD cells release less exosomes and show a loss in directional migration. (A) Exosomes were purified from differentiated control (NSshRNA), Rab27a shRNA (sh1; sh3), or SMPD2 shRNA (sh2; sh4) KD cells after treatment with fMLP (2 nM, 30 min) and analyzed using a bead-based flow cytometry assay with CD63-FITC, CD81-PE, and CD11b-APC conjugated antibodies. Panels show quantitative analysis from 3 independent experiments as mean ± SD. Evaluation of exosome flow cytometry was done as described in the legend of S2A Fig. See S4B Fig for flow cytometry graphs. **(B, C)** Exosomes were purified from differentiated control and shRNA KD cells stimulated with 2 nM fMLP. The exosomes were lysed and their LTB$_4$ content measured by EIA. Results from 3 independent experiments are shown as mean ± SD in pg/ml/10^8 cells (**B**) or pg/ml/μg of exosome protein (**C**). *** and NS indicate $p < 0.0001$ and $p > 0.05$, respectively, compared to corresponding control PLB-985 cells. **(D)** Differentiated control and shRNA KD cells were stimulated with subsaturating (1 nM) or saturating (1 μM) fMLP for 10 min, and the amount of LTB$_4$ in the supernatant was assessed by EIA. Results from 3 independent experiments are shown as mean ± SD. The symbols ** and *** indicate $p < 0.001$ and $p < 0.0001$, respectively, compared to corresponding NSshRNA controls. **(E)** EZ-Taxiscan chemotaxis towards 1 nM of control and KD cell lines. Corresponding migration speeds and CI were calculated from 4 different experiments and represented as mean ± SD. See legend of Fig 3E for details. Also see S8 Movie. **(F)** Differentiated NSshRNA, Rab27a, or SMPD2 KD cells or PLB-985 cells overexpressing LTB$_4$R1 were plated on fibronectin-coated plates for 10 min and uniformly stimulated with 1 nM fMLP. At specific time points, samples were subjected to western analyses using an antibody against pMLCII and total MLCII. Data are representative of 3 independent experiments. See S4C Fig for quantification. Raw data for panels A–D can be found in the Supporting information section S1 Data file. Uncropped blots for panel F can be found in the S1 Raw images file. CI, chemotaxis index; fMLP, N-formylMethionyl-Leucyl-Phenylalanine; KD, knockdown; LTB$_4$, leukotriene B$_4$; MLCII, myosin light chain II; NS, not significant; NSshRNA, nonspecific shRNA; pMLCII, phosphorylated MLCII; shRNA, small hairpin RNA.

https://doi.org/10.1371/journal.pbio.3001271.g004

and tracked their movement as they chemotaxed towards fMLP using the under agarose assay. To quantify the data, we color-coded the displacement tracks as a function of the imaging time; blue representing the cell's position during initial periods of migration and red the final. We found that compared to control cells (Fig 5Ai; S10 Movie), MK886-treated cells migrated shorter distances and with less direction, although speed of migration was not affected (Fig 5Aii; S10 Movie). We also found that treatment with GW4869, an nSmase inhibitor and a known inhibitor of exosome production [29] (S6A Fig), similarly affected chemotactic motion (Fig 5Bi and 5Bii; S11 Movie). Furthermore, and consistent with the chemotaxis defect of SMPD2 KD cells using the EZ-Taxiscan system (Fig 4E), we observed a similar loss in CI and distance migrated in SMPD2 shRNA KD cells (S6B Fig). We then asked if these defects could be rescued by the paracrine action of an exogenous source of exosomes. For this purpose, we mixed untreated neutrophils (labeled green) and treated (MK886 or GW4869) neutrophils (labeled red) in equal proportion and recorded their motility towards fMLP. We observed a dramatic improvement of both directionality and total distance migrated in MK886- (Fig 5Aiii; S10 Movie) and GW4869-treated neutrophils (Fig 5Biii; S11 Movie). No difference was found in the motility of untreated cells labeled either with the green or red dyes (Fig 5Ai, 5Aiv, 5Bi and 5Biv), excluding any dye-specific effects. Furthermore, NSshRNA cells similarly rescued the directionality defect of SMPD2 shRNA KD cells (S6B Fig).

While we observed a dramatic improvement in the CI of GW4869- or MK886-treated cells through the paracrine effects of exosomal LTB$_4$ (Fig 5A and 5B), we noticed that the treated cells showed defects in the time required to migrate towards fMLP (Fig 5C). It required up to 35 min for cells treated with either drug to traverse 300 μm, compared with 20 min for untreated cells (Fig 5A and 5B). In addition, the treated cells exhibited slower speeds as well as a loss of directional persistence in the initial phases of migration (Fig 5C). These defects in migration initiation and sensitization to a chemoattractant cue highlight a key role for exosomal LTB$_4$ in autocrine signaling.

One may argue that exosomal LTB$_4$ merely increases the robustness of the chemotactic response by regulating the cellular machinery as opposed to acting as a chemotactic beacon. We tested this by mixing cells that cannot detect fMLP with cells defective in exosome release and observed their migration towards fMLP. Due to their higher sensitivity to LTB$_4$, we used LTB$_4$R1 overexpressing cells as receiving cells in these experiments (Fig 4F). We treated green-labeled LTB$_4$R1 cells with the FPR-1 antagonist cyclosporin H (CsH) [30] and mixed them with red-labeled cells expressing control shRNA (NSshRNA), which were also treated with CsH. These cells did not migrate towards fMLP, confirming the efficacy of the antagonist treatment, and no such defects were observed when control labeled cells were mixed (Fig 6A).
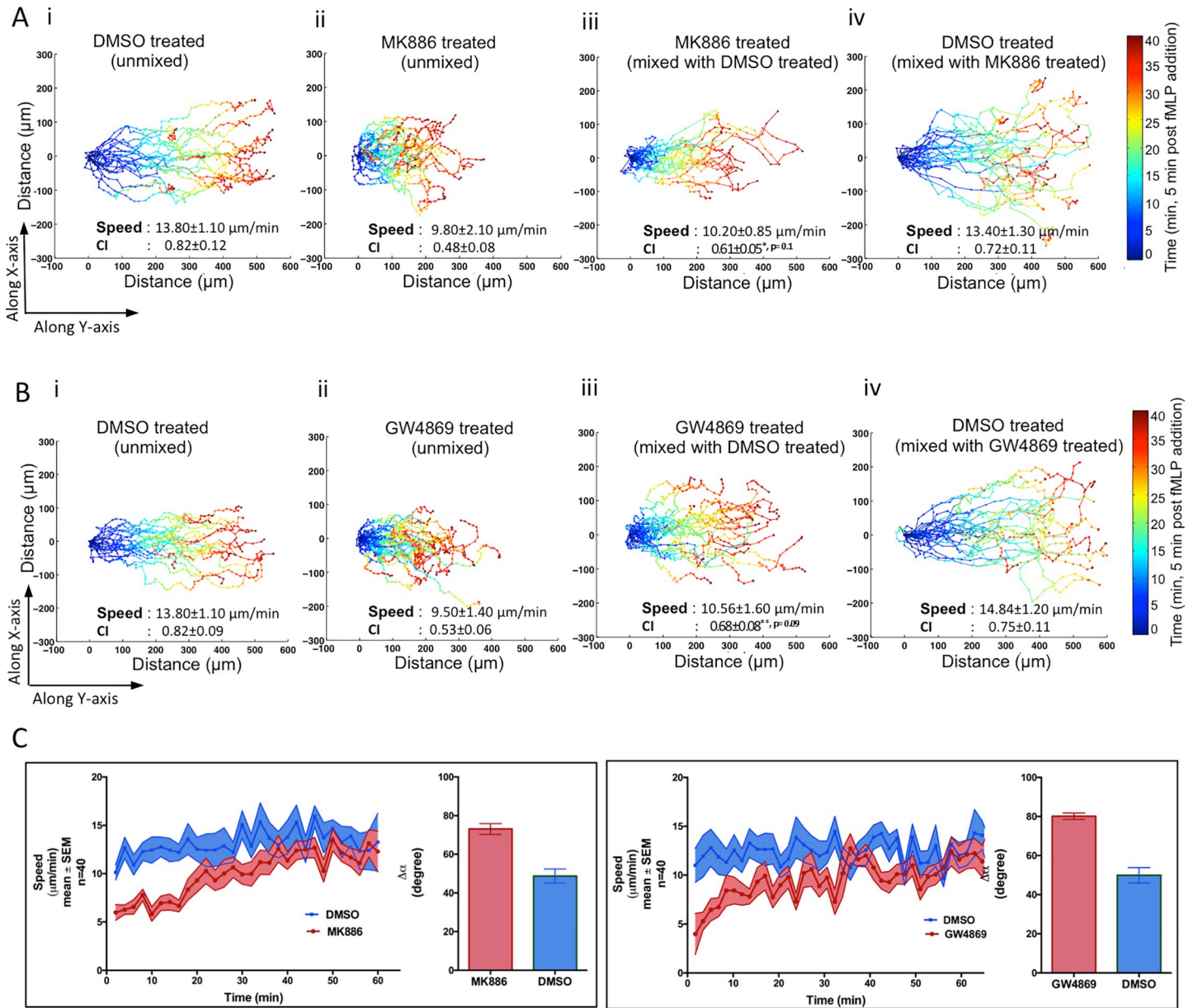
Fig 5. Exosomes mediate the paracrine and autocrine effects of LTB$_4$. (A) Cell tracks of neutrophils chemotaxing towards an approximately 50 pM/μm gradient of fMLP under agarose (see Materials and methods). **(i)** DMSO-treated cells stained with cytotracker red. **(ii)** MK886-treated cells stained with cytotracker red. **(iii, iv)** MK886-treated cells stained with cytotracker red mixed with DMSO-treated cells stained with cytotracker green: **(iii)** shows the tracks of MK886-treated red cells in the mixture, and **(iv)** shows tracks of DMSO-treated green cells in the mixture. Speed and CI were calculated from the tracks of 40 cells and averaging over 6 independent movies. The temporal location of cells in the X or Y direction is coded according to the color map shown. Also see S10 Movie. **(B)** Cell tracks of neutrophils chemotaxing towards fMLP as described in legends of A. In this case, neutrophils were treated with GW4869. Red cells were tracked in panels i–iii. In panel iv, DMSO-treated cells stained with cytotracker green were tracked. Speed and CI were calculated from the tracks of 40 cells and averaging over 6 independent movies. Also see S6B Fig and S11 Movie. **(C)** Graphs depicting the change in the speed of control- (labeled blue) or inhibitor- (labeled red) treated cells as a function of time. The mean average change in the angular deviation (Δα) between 2 consequent tracks in presented in the bar graph. Data were calculated by from the tracks of 40 cells and averaging over 6 independent movies. *** indicates $p < 0.0001$ compared to DMSO treated cells. Raw data for panels A–C can be found in the Supporting information section S1 Data file. CI, chemotaxis index; fMLP, N-formylMethionyl-Leucyl-Phenylalanine; LTB$_4$, leukotriene B$_4$.

https://doi.org/10.1371/journal.pbio.3001271.g005

However, the motility defect of CsH-treated LTB$_4$R1 cells was readily rescued when mixed with untreated NSshRNA cells, but not with MK886-treated NSshRNA cells (Fig 6B). These findings reiterate that LTB$_4$ released by NSshRNA cells is responsible for the *trans*-recruitment
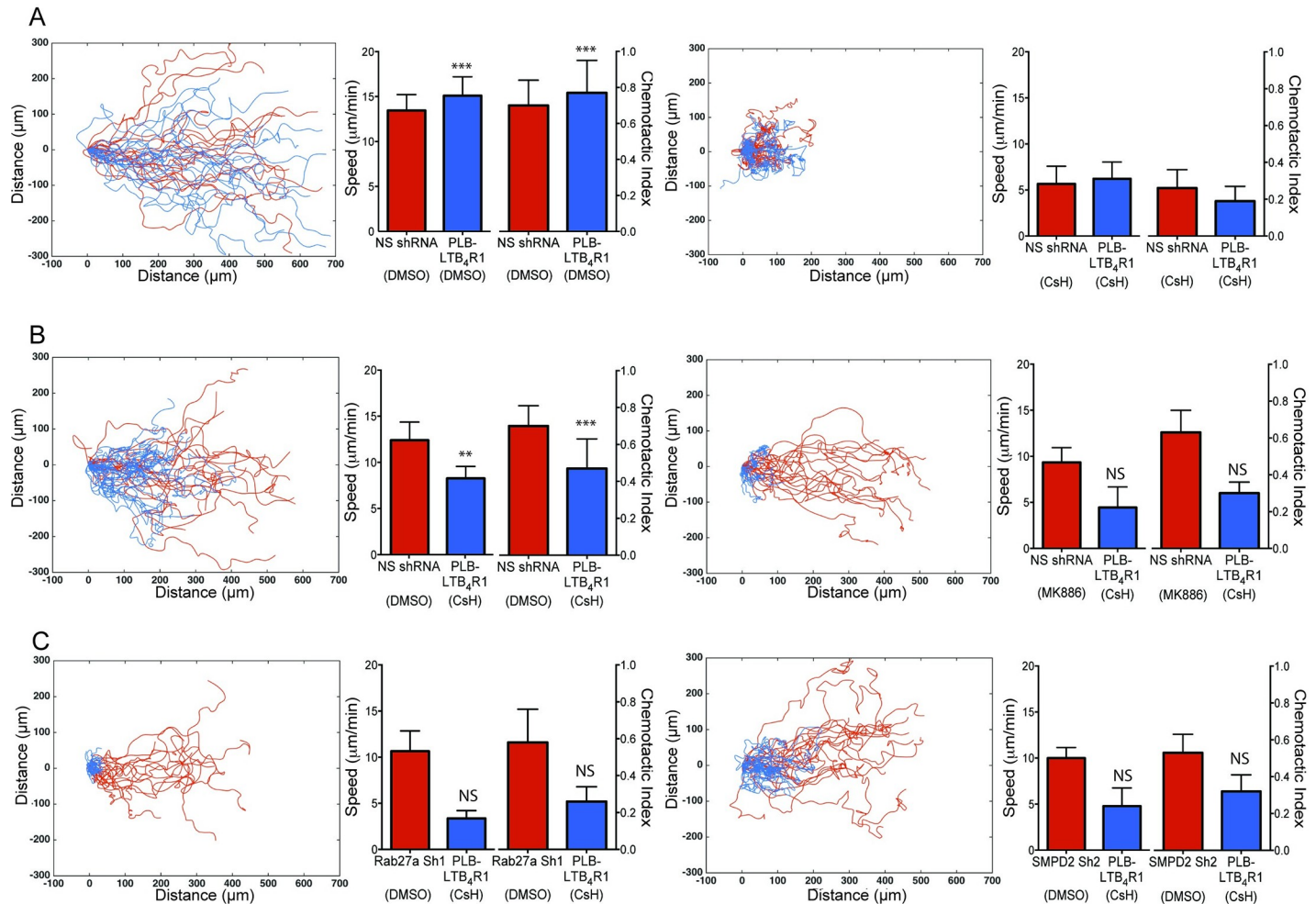
Fig 6. Exosomes mediate signal relay during neutrophil chemotaxis. Tracks, speed, and CI of mixtures of cytotracker-labeled cell lines migrating under agarose towards an approximately 50 pM/μm gradient of fMLP. Also see S7 Fig and S12 Movie. **(A)** Differentiated cells overexpressing the LTB$_4$R1 (labeled with cytotracker green, shown as blue tracks) in a mixture with NSshRNA cells (labeled with cytotracker red, shown as red tracks) treated with DMSO (left) or CsH (right). Composite graph shows displacement tracks of both types of cells. Speed and CI were calculated from the tracks of 40 cells and averaging over 8 independent movies. **(B)** Differentiated cells overexpressing the LTB$_4$R1 (labeled with cytotracker green, shown as blue tracks) treated with CsH in a mixture with NSshRNA cells (labeled with cytotracker red, shown as red tracks) treated with DMSO (left) or MK866 (right). Composite graph shows displacement tracks of both types of cells. Speed and CI were calculated from the tracks of 40 cells and averaging over 4 independent movies. **(C)** Differentiated cells overexpressing the LTB$_4$R1 (labeled with cytotracker green, shown as blue tracks) in a mixture with Rab27a sh1 (labeled with cytotracker red, shown as red tracks) or SMPD2 sh2 (right) cells treated with DMSO. Composite graph shows displacement tracks of both types of cells. Speed and CI were calculated from the tracks of 40 cells and averaging over 4 independent movies. The symbols ***, **, *, and NS indicate $p < 0.0001$, $p < 0.001$, $p < 0.01$, and $p > 0.05$, respectively, compared to CsH-treated PLB-LTB$_4$R1 cells. Raw data for panels A–C can be found in the Supporting information section S1 Data file. CI, chemotaxis index; CsH, cyclosporin H; fMLP, N-formylMethionyl-Leucyl-Phenylalanine; LTB$_4$R1, receptor for LTB$_4$; NS, not significant; NSshRNA, nonspecific shRNA.

of CsH-treated cells. Importantly, no rescue in motility was observed in CsH-treated LTB$_4$R1 cells when they were mixed with Rab27a or SMPD2 KD cells (Fig 6C) and in GW4869- or MK866-treated neutrophils (S7 Fig). Together, these observations indicate that exosomal LTB$_4$ relays chemotactic signals in response to primary attractants during neutrophil chemotaxis.

Discussion

Our prior studies on neutrophil migrating in chemotactic gradients identified LTB$_4$ as an important signal relay molecule that increases the recruitment range of neutrophils to sites of
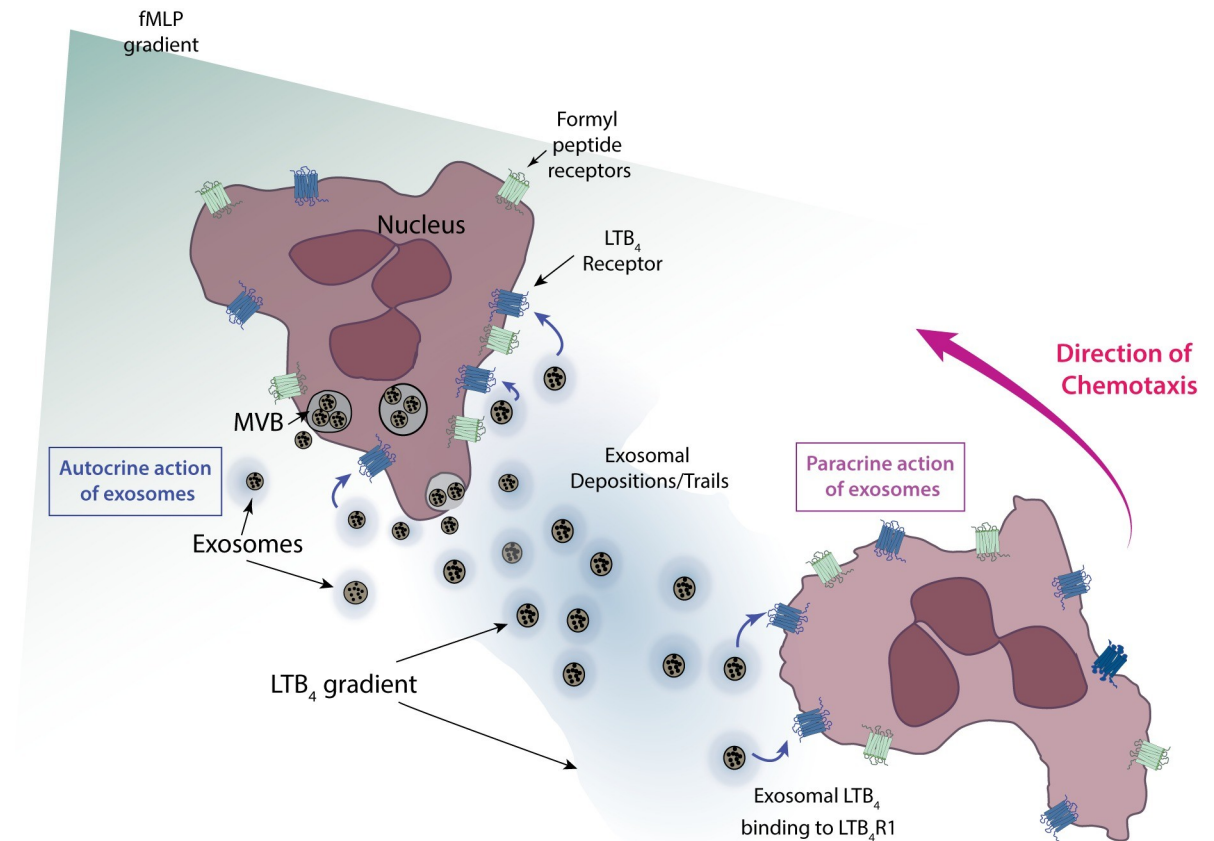
Fig 7. Illustration depicting exosome mediated LTB$_4$ relay in neutrophils chemotaxing to fMLP. Cartoon depicting 2 neutrophils chemotaxing toward an fMLP gradient (green). LTB$_4$ released from exosomes are shown in blue. See text for details. fMLP, N-formylMethionyl-Leucyl-Phenylalanine; LTB$_4$, leukotriene B$_4$; LTB$_4$R1, receptor for LTB$_4$; MVB, multivesicular body.

https://doi.org/10.1371/journal.pbio.3001271.g007

inflammation [7,12]. This observation led us to study the mode of LTB$_4$ release from cells and its effective dissemination. In this study, we show that LTB$_4$ is packaged in MVBs that are released as exosomes during neutrophil chemotaxis. We present this as a mechanism through which hydrophobic low-diffusible lipid molecules, like LTB$_4$, mediate the signal relay process. Our study proposes that neutrophils migrating in primary chemoattractant gradients release exosomes containing LTB$_4$ and LTB$_4$ synthesizing enzymes. These exosomes subsequently act in an autocrine manner—by sensitizing cells towards the primary chemoattractant—and in a paracrine manner—by acting as molecular beacons for following cells (Fig 7).

We found that both LTB$_4$ and 5-LO are present in exosomes, which also contain LTA$_4$H and FLAP. The presence of LTB$_4$ synthesizing enzymes has previously been reported in exosomes derived from macrophages and dendritic cells [31]. However, unlike dendritic cells that constitutively produce exosomes [32], we detected little or no release of exosomes in unstimulated neutrophils. Instead, we observed exosome release upon treatment with ionomycin as well as following the addition of fMLP, but not GM–CSF, indicating that exosome release is a result of primary stimulation and not a priming event. fMLP is also known to increase the release of plasma membrane–derived secretory vesicles and ectosomes [33] that have considerable overlap with exosomes in terms of size (50 to 200 nm). However, owing to their differences in lipid composition [34], we were able to separate exosomes from ectosomes using iodixanol density gradients. Moreover, the purified exosomes were able to activate resting

neutrophils, indicating proinflammatory responses compared to the reported anti-inflammatory responses of ectosomes [33]. Finally, using Rab27a and SMPD2 KD cells, we established that exosomes represent the primary pathway for LTB$_4$ release in chemotaxing neutrophils under physiological stimulation conditions. Impaired neutrophil recruitment has been observed in Rab27a knockout (KO) mice under in vivo neutrophil recruitment models [35]. Furthermore, neutrophils deficient in vesicle fusion show less migration in vitro and in an in vivo model of gout [36]. The migration defects we observed in Rab27a and SMPD2 KD cells therefore provide valuable mechanistic insights into the migration defects observed in vivo. Furthermore, the docking of 5-LO containing MVBs at the back of cells and the subsequent release of exosomes are reminiscent of the molecular beacon model first shown in chemotaxing *Dictyostelium* cells [18]. This is similar to recent in vivo observations made by Sung and colleagues [37], where exosome released by HT1080 cells bind to integrins and act as adhesion trails for cellular guidance.

Under uniform stimulation conditions, exosomal LTB$_4$ levels range from 2 to 10 nM and are sufficient to elicit neutrophil migration in chemotaxis assays. This, however, may not reflect the actual amount of LTB$_4$ being released from exosomes during chemotaxis for the following reasons: (i) exosome release is fMLP dose-dependent and hence a function of the primary chemoattractant gradient; (ii) purified exosomes were prepared by uniformly stimulating neutrophils with subsaturating fMLP concentrations and losses incurred during the purification processes could lead to underestimated amounts of exosomes recovered; (iii) the rate of LTB$_4$ release from exosomes and the effective LTB$_4$ gradient across and between cells cannot be reliably measured in real time due to the lack of sensitive methodologies; and (iv) the presence of the LTB$_4$ synthesizing enzymes, 5-LO, LTA$_4$H, and FLAP in neutrophil exosomes along with the presence the primary substrate AA [38], suggest active exosomal LTB$_4$ synthesis. Indeed, exosomes isolated from dendritic cells are capable of synthesizing AA metabolites [31]. Although our study elucidates the trafficking and secretion of LTB$_4$ during neutrophil chemotaxis, the mechanisms regulating the release of exosomal LTB$_4$ remain to be determined. These may include membrane diffusion, passive or active lysis through released neutrophil proteases, or through docking to cell surface heparan sulfate proteoglycans [39]. Alternatively, active LTB$_4$ release may be mediated through ABC transporters [40] or other types of active processes. The availability of methods that are sensitive and, most importantly, capable of measuring LTB$_4$ in real time and space will help elucidate how LTB$_4$ gradients are established and propagated during neutrophil chemotaxis.

Our findings show that exosomal LTB$_4$ regulates neutrophil chemotaxis in an autocrine and paracrine fashion. First, we found that Rab27a and SMPD2 KD cells as well as neutrophils treated with an nSmase inhibitor exhibit profound defects in directionality and recruitment range towards fMLP. Similar defects were observed in neutrophils derived from Rab27a KO mice [35] and were primarily attributed to granule exocytosis, a process that is closely related to exosome biogenesis and release. Chemotaxis has not been studied in neutrophils isolated from SMPD2 KO mice, although its role may be inferred through the effects of GW4869 on neutrophil migration. GW4869 did not inhibit neutrophil speed but abrogated directional migration towards fMLP [41], an observation that mirrors our own observation with GW4869 and SMPD2 KD cells. Second, we found that the defects in directionality and recruitment range of SMPD2 KD as well as GW4869-treated cells are rescued by the presence of control cells that provide exosomes to relay signals. One could argue that the rescue was simply due to supplementation of ceramide from the released exosomes and not related to LTB$_4$ content [41]. However, we observed a very similar phenotypical recovery by inhibiting LTB$_4$ synthesis alone. More importantly, unlike control cells, the KD cells were unable to send a paracrine

signal to neutrophils with blocked FPR1, clearly establishing that exosomes represent a critical bearer of the signal relay message.

Exosomes are well-established mediators of intercellular communication [42] and have been known to mediate cell migration in various systems [37]. This work establishes that exosomal communication is extremely efficient and critical in fast moving cells and occurs at a faster rate compared to the slow constitutive release of exosomes reported in the literature [28]. Moreover, our findings add valuable insight into the mechanisms that underlie chronic inflammatory conditions, such as asthma and rheumatoid arthritis [43], as well as lung cancer progression [44], where LTB$_4$ plays a central role. We envision that the secretion of other signals that foster communication between cells in harsh extracellular environments are similarly processed through exosome packaging.

Materials and methods

Ethics statement

Heparinized whole blood from anonymous healthy human donors was obtained by venipuncture from the NIH Blood Bank Research Program (https://clinicalcenter.nih.gov/blooddonor/donationtypes/lab_research.html) or from the Platelet Pharmacology and Physiology Core at the University of Michigan (IRB#HUM00107120). In both cases, the samples were deidentified, and we did not have access to the HIPAA information.

Materials

OptiPrep, Histopaque 1077, fMLP, IL8, and LY294002 were obtained from Sigma-Aldrich (St. Louis, Missouri). LTB$_4$, MK886, and LY223982 were purchased from Cayman Chemical (Ann Arbor, Michigan). Anti-5-LO, anti-p-Akt (clone C31E5E for S473), anti-AKT, anti-MLCII, anti-pMLCII (Ser19), anti-total ERK1/2, and anti-p-Erk1/2 (clone D13.14.4E) rabbit antibodies were all purchased from Cell Signaling Technology (Beverly, Massachusetts). Anti-MMP9, anti-myeloperoxidase, anti-CD63, anti-LAMP1, and anti-GM130 were obtained from Abcam (Cambridge, Massachusetts). CD11b APC antibody was purchase from BD Biosciences (San Jose, California).

Isolation of human peripheral blood neutrophils

Heparinized whole blood was obtained by venipuncture from healthy donors. Neutrophils were isolated using dextran sedimentation (3% dextran/0.9% NaCl) coupled to differential centrifugation over Histopaque 1077 [45]. Residual erythrocytes were removed using of hypotonic lysis with 0.2% and 1.6% saline solutions.

Cell lines

HEK293T cells (ATCC, Manassas, Virginia, United States of America) and Phoenix cells (Orbigen, San Diego, California) were maintained as previously described [46]. For virus packaging, 80% confluent cells were used for transient transfection using Lipofectamine reagent according to manufacturer's protocol (Life Technologies). PLB-985 cells were maintained in an undifferentiated state and differentiated as described [46]. The status of differentiation was monitored by Mac-1 staining.

Plasmid constructs and infections of PLB-985 cells

PLB985 cells expressing mCherry-5LO and CD63-GFP as well as co-expressing both CD63-GFP and mCherry-5LO were created using a retroviral approach. Rab27a and SMPD2 KD were achieved using the pGIPZ lentiviral system (GE Dharmacon).

Constructs and infections of PLB-985 cells

Retroviral approach. The mCherry gene was amplified from pCDNA3.1-mCherry, cloned at the 5′ end of the 5-LO cDNA and introduced in pMSCV-Puro. Similarly, eGFP was amplified from pEGFP-N1, cloned at the 3′ end of the CD63 cDNA (kindly donated by Dr. Paul Roche (NIH)), and introduced in pMSCV-Neo. Stable cell lines were created as described [46]. Briefly, expression plasmids were transfected along with the helper plasmid pVSV-G into the packaging Phoenix cell line using Lipofectamine 2000. Transiently produced viruses were harvested after 48 or 72 h. PLB-985 cells were infected with the virus with fresh RPMI1640 culture medium containing 4 μg/ml polybrene and incubated for an additional 48 h. Cells stably expressing the genes were selected in media containing 1.6 mg/ml G-418 or 0.8 μg/ml Puromycin. Stable clonal populations were generated after 14 to 21 d and maintained in the selection media. mCherry-5LO containing pMSCVneo was similarly infected into PLB-985 cells expressing CD63-GFP to create cells co-expressing CD63-GFP and mCherry-5LO.

Lentiviral approach. Undifferentiated PLB-985 cells were infected with pGIPZ shRNA lentiviruses (GE Dharmacon) carrying the following hairpin sequence using the manufacturer's recommendations:

Accession	shRNA Name	Hairpin
XM_005267109	SMPD2 shRNA1	TGCTGTTGACAGTGAGCGCCGCCGTTGATGTGTGTGCTAATAGTGAAGCCACAGATGTATTAGCACACACATCAACGGCGATGCCTACTGCCTCGGA
XM_005267109	SMPD2 shRNA2	TGCTGTTGACAGTGAGCGCAGGCAACACAATGGTACCCAATAGTGAAGCCACAGATGTATTGGGTACCATTGTGTTGCCTTTGCCTACTGCCTCGGA
NM_003080	SMPD2 shRNA3	TGCTGTTGACAGTGAGCGAGGGGACAGAACTAAAGAACAATAGTGAAGCCACAGATGTATTGTTCTTTAGTTCTGTCCCCCTGCCTACTGCCTCGGA
XM_005267109	SMPD2 shRNA4	TGCTGTTGACAGTGAGCGCCCGCATTGACTACGTGCTTTATAGTGAAGCCACAGATGTATAAAGCACGTAGTCAATGCGGATGCCTACTGCCTCGGA
NM_003080	SMPD2 shRNA 5	TGCTGTTGACAGTGAGCGATGGGTTTTACATCTCCTGTAATAGTGAAGCCACAGATGTATTACAGGAGATGTAAAACCCAGTGCCTACTGCCTCGGA
NM_004580	Rab27a shRNA1	TGCTGTTGACAGTGAGCGCGCTCAATGTCTTTGAGTATTATAGTGAAGCCACAGATGTATAATACTCAAAGACATTGAGCTTGCCTACTGCCTCGGA
NM_183236	Rab27a shRNA2	TGCTGTTGACAGTGAGCGAGCCCAGAGTCTTACATTTAAGTAGTGAAGCCACAGATGTACTTAAATGTAAGACTCTGGGCCTGCCTACTGCCTCGGA
NM_004580	Rab27a shRNA3	TGCTGTTGACAGTGAGCGCGGCTGCAGCTTTATTAGCTTATAGTGAAGCCACAGATGTATAAGCTAATAAAGCTGCAGCCTTGCCTACTGCCTCGGA
XM_005254577	Rab27a shRNA4	TGCTGTTGACAGTGAGCGCCCAGTGTACTTTACCAATATATAGTGAAGCCACAGATGTATATATTGGTAAAGTACACTGGTTGCCTACTGCCTCGGA
NM_183234	Rab27a shRNA5	TGCTGTTGACAGTGAGCGCAGGGAAGACCAGTGTACTTTATAGTGAAGCCACAGATGTATAAAGTACACTGGTCTTCCCTATGCCTACTGCCTCGGA
NM_183236	Rab27a shRNA6	TGCTGTTGACAGTGAGCGAATGCCTCTACGGATCAGTTAATAGTGAAGCCACAGATGTATTAACTGATCCGTAGAGGCATGTGCCTACTGCCTCGGA

Rab27a shRNA1 (sh1), Rab27a shRNA3 (sh3), SMPD2 shRNA2 (sh2), and SMPD2 shRNA 3 (sh4) were selected for further studies based on their ability to KD both mRNA and protein levels of their respective target genes. pGIPZ nonsilencing lentiviral shRNA control was obtained from GE Dhramacon.

Exosome isolation

A total of 5×10^8 cells were primed with GM–CSF (5 ng/ml; R&D Systems) for 30 min in RPMI without phenol red containing 5% FBS and 10 mM HEPES, centrifuged and resuspended in ice-cold PBS for 30 min to reduce basal exocytosis levels. Cells were harvested and resuspended in modified HBSS (mHBSS) with or without 2 nM fMLP for 30 min at 37˚C and centrifuged at 500xg for 5 min. To assess the exosome producing ability of various stimulants, unprimed cells were resuspended in basal buffer (25 mM HEPES (pH 7.4), 140 mM NaCl, 4.7 mM KCl, 1.4 mM MgCl$_2$, and 10 mM glucose) and stimulated for 30 min with either ionomycin (1 μM) supplemented with CaCl$_2$ (2 mM), fMLP (1 μM), GM–CSF (5 ng/ml), or DMSO (0.1%). The supernatant was further centrifuged at 2,000xg for 20 min. The resulting supernatants were filtered twice through low protein binding 0.45 μm filters and subsequently centrifuged at 100,000xg for 60 min at 4˚C. The recovered pellet, containing a heterogeneous mixture of crude vesicles, was resuspended in 500 μl PBS. Further purification of the exosomes was performed as previously reported [47]. Briefly, the resuspended vesicles were loaded onto a discontinuous gradient of iodixanol (40%, 20%, 10%, and 5%, w/v solutions in 0.25 M sucrose/10 mM Tris (pH 7.5)) and centrifuged at 100,000xg for 18 h at 4˚C. Fractions were collected, diluted in PBS, and centrifuged at 100,000xg. The pellet was washed in PBS, and the recovered fractions were used as described.

Flow cytometric analysis of exosomes

Purified exosomes were incubated with 3.9 μm diameter aldehyde/sulfate latex beads (Life Technologies) for 15 min at room temperature (RT) followed by the addition of 10 μg BSA for an additional 15 min. The incubation volume as increased to 250 μl in PBS and incubated overnight on a turnover rocker. The incubation was stopped the following day by adding glycine to a final concentration of 100 mM. The exosomes-coated beads were washed twice in FACS wash (3% FCS and 0.1% NaN$_3$ in PBS) and resuspended in 400 μl FACS wash. The beads were incubated for 30 min with each conjugated primary antibody, washed and analyzed on a FACSCalibur flow cytometer (BD Biosciences). Bead-based flow cytometry was also performed with CD63 antibody-coated dynabeads according to manufacturer's protocol (Invitrogen).

Subcellular fractionation through nitrogen cavitation

Freshly isolated neutrophils (50×10^6) were incubated with DFP for 15 min at 37˚C, pelleted and resuspended in 1X disruption buffer (DB; 100 mM KCl, 3 mM NaCl, 3.5 mM MgCl$_2$, 1.5 mM EGTA, and 10 mM 1,4-piperazinediethanesulfonic acid (PIPES) (pH 7.2), including 1 mM sodium salt of ATP and 0.5 M PMSF) with or without 2 nM fMLP. The reaction was stopped after 2 min by adding an equal volume of ice-cold DB. Cavitation was carried out for 5 min at 500 psi on ice. Cavitates were collected and EGTA was added to the final concentration of 1.5 mM. Lysed cells were centrifuged at 400xg for 20 min to remove cell debris and nuclei and 15,000xg for 15 min to remove mitochondria. The supernatant was then top loaded onto a 5% to 30% continuous OptiPrep gradient prepared by appropriately diluting a 60% optiprep stock with 3X DB. The gradient was centrifuged at 34,000xg for 18.5 h, and 1 ml fractions were collected. Fractionates <1.04 g/l containing primarily cytosolic fraction was discarded and the rest analyzed by immunoblotting after trichloroacetic acid (TCA) precipitation. To determine the density of each fraction, a control OptiPrep gradient containing a blank containing DB was run in parallel. Fractions were collected as described, serially diluted 1:10,000 with water, and the iodixanol concentration determined by absorbance at 244 nm using a molar extinction coefficient of 320 L g^{-1}cm^{-1}.

Chemotaxis assays

Chemotaxis was assessed using the under-agarose assay or the EZ-Taxiscan as previously described [46,48].

Under-agarose assay. Cell culture dishes were coated with 0.2% gelatin in PBS for 1 h at 37˚C. Agarose (0.5%) in 50% PBS and 50% mHBSS was poured and allowed to solidify for 40 min. Three 1 mm diameter wells were carved at 2 mm distance from each other. A chemoattractant was placed in the middle well 15 min before plating neutrophils. The chemoattractant concentration achieved using this method was assessed as described by Afonso and colleagues [7]. Typically, a gradient of 50 pM/µm fMLP was used for under-agarose assays. A total of 5×10^5 neutrophils in 5 µL mHBSS were plated in the outer wells and incubated at 37˚C. Cells were allowed to chemotax for 30 min to 2 h depending on the experimental requirement. Cells migrating under agarose were imaged using Axiovert 200 (Carl Zeiss) equipped with a confocal system (Ultraview ERS; PerkinElmer) with a spinning disk head (Yokogawa) Single plane images and z stacks were taken using 63 and 100× plan neofluor objectives (Carl Zeiss).

EZ-Taxiscan assay. The EZ-Taxiscan chamber (Effector Cell Institute, Tokyo, Japan) was assembled as described by the manufacturer. Cell migration was recorded every 15 s for 45 min at 37˚C in a humidified environmental chamber. Coverslips and chips used in the chamber were coated with 1% bovine serum albumin at RT for 1 h. All glass coverslips were ultrasonicated and washed before use. Cell migration analysis was conducted using MATLAB software as previously described [46].

Adhesion assay. Cells (5×10^5 cells/well) were plated on 96-well plates coated with fibronectin, stimulated for 30 min at 37˚C, shaken at 2,000 RPM (radius = 1 cm) for 10 s on an orbital shaker, and unbound cells were removed. The remaining cells were fixed (4% PFA) and stained with crystal violet 5 mg/mL in 2% ethanol. Crystal violet was extracted by the addition of 2% SDS, and absorbance was measured at 570 nm.

Negative stain preparation and electron microscopy

Exosome preparations were prepared for negative stain EM using established methods [49]. In brief, 200-mesh copper grids covered with carbon-coated collodion film (EMS, Hatfield, Pennsylvania, USA) were glow discharged for 30 s at 10 mA in a PELCO easiGlow glow discharge unit (Fresno, California, USA). Aliquots (3.5 µl) of the exosome preparations were adsorbed to the grids and incubated for 1 min at RT. Samples were then washed with 2 drops of water and stained with 2 successive drops of 0.7% (w/v) uranyl formate (EMS, Hatfield, Pennsylvania, USA) followed by blotting until dry. Samples were visualized on a Morgagni 100 kV transmission electron microscope (Thermo Fisher Scientific, Waltham, Massachusetts, USA) at −1.5 µm defocus value.

Data analysis and diameter measurements

Images were downloaded in JPG format and opened in ImageJ [50]. To perform diameter measurements, a spatial scale of the active image was defined by measuring a 50-nm scale bar on a single micrograph with the *set scale* function. Diameter measurements for each dataset were made using a line tool followed by the *measure* function. A total of 200 measurements were made for each dataset.

Nanoparticle tracking analysis

The Malvern Nanosight NS300 equipped with 488 nm laser, a high sensitivity sCMOS camera, and syringe pump was used to capture the data for nanoparticle tracking analyses, which were

analyzed using the NTA 3.3 Dev Build 3.3.301 software. The purified exosomes were resuspended in 10 mM Tris-Cl (pH 7.4) with 250 mM sucrose, mixed by vortexing, and diluted to 1:100 in particle-free water (0.22 μm filtered) to obtain a concentration within the recommended measurement range (1 to 10×10^8 particles/mL). Using a syringe pump speed of 100/ AU, the videos of the particles inflow were captured in script control mode, as 5 videos of 60 s each with 1 s delay and viscosity of water at 25˚C. The camera level was kept at 14, capturing 25 frames/s with a total acquisition of 1,500 frames/sample.

Mixed cell chemotaxis assay, image acquisition, and motility analysis

Cytotracker dyes were added to differentiated PLB-985 cells or freshly isolated neutrophils according to manufacturer's protocol (Life Technologies), washed and resuspended in mHBSS containing appropriate inhibitors/antagonists. Cells were then washed, and 2.5×10^5 cells of differently labeled cells were mixed. These cells were resuspended in 5 μl mHBSS and loaded onto an under-agarose chamber. Time-lapse imaging was performed using a Plan-Neofluar 10x/0.30 objective (Zeiss Axiovert S100 microscope). Cell tracks were extracted and analyzed using a method developed by McCann and colleagues [51] supplemented by tracking through ImageJ. CI and Δα (persistance) were used to analyze motility behavior. CI was calculated by taking the cosine of the angle between the final displacement vector and the line connecting the chemotactic source to the initial position of the cell. A value of 1 designates perfect chemotaxis. Δα is measured through the angular change between the displacement vector at any given time and the preceding displacement vector. Larger Δα designates lower persistence.

LTB$_4$ measurements

Total LTB$_4$ levels were measured using an ELISA kit (R&D Systems). Briefly, neutrophils or PLB-985 cells were resuspended at 1×10^6 cells/ml in PBS and incubated for 30 min on ice. GM–CSF (5 ng/ml; R&D Systems) was added, and cells were further incubated for 1 h at 37˚C, centrifuged at 400xg for 5 min, resuspended in a volume of 200 μl at 24×10^6 cells/ml in RPMI, and incubated at 37˚C until stimulated. The reactions were stopped by adding cold PBS. Cells were centrifuged and LTB$_4$ in supernatants were assayed according to manufacturer's instructions. Exosomal LTB$_4$ was measured using the EIA kit according to manufacturer's protocol (Cayman Chemicals) after disruption by sonication. To measure LTB$_4$ in the vesicular fractions of lysed neutrophils, total lipids were first extracted from the different fractions using a method outlined by McColl and colleagues [52]. The extracted lipids were acidified to pH 4.0, loaded onto a C18 SPE column, and eluted with ethyl acetate containing 10% methanol, evaporated under inert nitrogen stream, and resuspended in buffer to obtain a concentrated pool of LTB$_4$. LTB$_4$ levels were measured using the EIA kit (Cayman Chemicals) according to manufacturer's recommendations.

Immunoblotting

Neutrophils were either resuspended in RPMI (1% bovine serum) or plated on fibronectin-coated chambers (for pMLCII) and incubated with inhibitors and diisopropyl fluorophosphates (DFPs) (2 mM) for 10 min at 37˚C. Cells were then stimulated with fMLP, collected at specific time points, lysed for 15 min in ice-cold lysis buffer (20 mM Tris (pH 7.5), 10 mN NaCl, 1 mM EDTA, 0.1% NP-40, 3 mM DFP, 2 mM orthovanadate, 10 g/mL aprotinin, 10 g/ mL leupeptin, 2.5 mM napyrophosphate, complete protease inhibitor cocktail (Roche Diagnostics, Indianapolis, Indiana)) and processed for SDS-PAGE analyses.

Supporting information

S1 Fig. Characterization of cells expressing CD63-GFP, mCherry-5LO, and CD63/5-LO.
(**A**) PLB-985 cells expressing CD63-GFP or mCherry-5LO were plated on fibronectin-coated
(50 µg/ml) coverslips, fixed with 4% paraformaldehyde, and imaged in the absence of fMLP.
Also see S1 Movie. (**B**) PLB985 cells expressing mCherry-5LO migrating under agarose
towards fMLP were fixed with 3.7% paraformaldehyde, 0.1% glutaraldehyde in 0.1 M cacody-
late buffer containing 320 mM sucrose, permeablized with 0.2% Triton-X100 for 2 min, and
counterstained with Phalloidin FITC. The slope of the gradient is approximately 50 pM/µm, as
previously assessed [7]. (**C**) Images of PLB985 cells expressing CD63-GFP migrating under
agarose towards fMLP. The slope of the gradient is approximately 50 pM/µm, as previously
assessed [7]. Images shown are representative of 6 independent experiments. CD63-GFP,
GFP-tagged CD63; fMLP, N-formylMethionyl-Leucyl-Phenylalanine; mCherry-5LO,
mCherry-tagged 5-LO.
(PDF)

S2 Fig. Characterization of exosomes released from resting and activated neutrophils. (A)
Exosomes were purified from neutrophils treated with increasing concentrations of fMLP and
their surface levels of CD11b assessed by bead-based flow cytometry. Percentage positivity
shown is based on the gated exosome fraction derived from nonstimulated cells. Inset:
Amount of purified exosomes is quantified by multiplying the percentage positivity of each
fraction from 4 independent experiments with corresponding relative median fluorescence
intensity values. (**B**) CD81 levels in exosomes purified from neutrophils treated with increas-
ing concentrations of fMLP assessed as mentioned in A. (**C**) CD81 levels in exosomes purified
from neutrophils treated with DMSO, Ionomycin, fMLP, and GM–CSF. (**D**) Quantitation of
exosome amounts were done as descried in A, using values from 3 independent experiments.
Raw data for panels A, B, and D can be found in the Supporting information section S2 Data
file. fMLP, N-formylMethionyl-Leucyl-Phenylalanine; GM–CSF, granulocyte macrophage–
colony-stimulating factor.
(PDF)

S3 Fig. Bioactivity of purified exosomes. (A) LTB$_4$ (10 nM) or exosomes isolated from PLB-
985 cells expressing either mCherry or mCherry-5LO (50 µg/ml) was added to neutrophils for
15 min, and pAkt (S473) and p44/42 MAPK (Erk1/2; T202/Y204) levels were measured using
specific antibodies. Quantification of 3 independent experiments is presented as the amount of
phosphorylated protein relative to that of DMSO-treated cells (mean ± SD). The amount of
pAkt or pErk1/2 at each point was standardized by dividing its value with the value of total
Akt or Erk1/2 at the same time point. (**B**) Neutrophils were treated with or without 10 µM
LY223982 for 30 min and allowed to migrate towards 1 µM fMLP. Data are representative of 3
independent experiments. See legend of Fig 3E for details. (**C**) Exosomal LTB$_4$ (see legends of
Fig 3G for details) derived from PLB-985 cells expressing mCherry, mCherry-5LO, or
CD63-GFP was added to neutrophils (pretreated or not with LY223982) for 15 min, and pAkt
(S473) levels were measured using specific antibodies. Quantification of 3 independent experi-
ments is presented as the amount of pAkt S473 after stimulation relative to that of unstimu-
lated cells (mean ± SD). The amount of pAkt S473 at each time point was standardized by
dividing its value with the value of total Akt of the same time point. Raw data for panels A–C
can be found in the Supporting information section S2 Data file. CD63-GFP, GFP-tagged
CD63; CI, chemotaxis index; fMLP, N-formylMethionyl-Leucyl-Phenylalanine; LTB$_4$, leuko-
triene B$_4$; mCherry-5LO, mCherry-tagged 5-LO.
(PDF)

S4 Fig. Characterization of Rab27a and SMPD2 KD cells. (A) Differentiated and undifferentiated PLB-985 cells were lysed and subjected to western analyses using antibodies specific for Rab27a and nSmase1. GAPDH levels were used as loading controls. Results are representative of 3 independent experiments. **(B)** Exosomes were purified from differentiated control (NSshRNA), Rab27a shRNA (sh1; sh3), or SMPD2 shRNA (sh2; sh4) KD cells after treatment with fMLP (2 nM, 30 min) and analyzed using a bead-based flow cytometry assay with CD63-FITC, CD81-PE, and CD11b-APC conjugated antibodies. See Fig 4A for quantification and additional details. **(C)** Differentiated NSshRNA, Rab27a or SMPD2 KD cells, or PLB-985 cells overexpressing LTB$_4$R1 were plated on fibronectin-coated plates for 10 min and uniformly stimulated uniformly with 1 nM fMLP. At specific time points, samples were subjected to western analyses using an antibody against pMLCII and total MLCII. Quantification of 3 independent experiments is presented as the amount of pMLCII after fMLP stimulation relative to that at time 0 (mean ± SD). Raw data for panel C can be found in the Supporting information section S2 Data file. Uncropped blots for panel A can be found in the S1 Raw images file. fMLP, N-formylMethionyl-Leucyl-Phenylalanine; GAPDH, glyceraldehyde 3-phosphate dehydrogenase; KD, knockdown; LTB$_4$R1, receptor for LTB$_4$; MLCII, myosin light chain II; NSshRNA, nonspecific shRNA; pMLCII, phosphorylated MLCII; shRNA, small hairpin RNA. (PDF)

S5 Fig. Response of Rab27a and SMPD2 KD cells to fMLP. (A) Differentiated PLB-985 Rab27a and SMPD2 KD cells were plated on fibronectin-coated (50 μg/ml) plates for 10 min and uniformly stimulated with 1 μM fMLP. The plates were then shaken, and the number of remaining cells attached to the plates was estimated by crystal violet staining. Results represent the percent average ± SD compared to PLB-985 control of 3 independent experiments. **(B)** Differentiated PLB-985, NSshRNA, Rab27a, and SMPD2 KD cells were uniformly stimulated with 100 nM fMLP, and pERK1/2 levels were assessed by immunoblotting. **(C)** EZ-Taxiscan chemotaxis towards 1 μM of control and KD cell lines. Corresponding migration speeds and CI were calculated from 4 different experiments and represented as mean ± SD. See legend of Fig 3E for details. Also see S9 Movie. Raw data for panel A can be found in the Supporting information section S2 Data file. Uncropped blots for panel B can be found in the S1 Raw images file. CI, chemotaxis index; fMLP, N-formylMethionyl-Leucyl-Phenylalanine; GAPDH, glyceraldehyde 3-phosphate dehydrogenase; KD, knockdown; NSshRNA, nonspecific shRNA. (PDF)

S6 Fig. Effect of SMPD2 KD on exosome production and neutrophil chemotaxis. (A) Exosomes purified from DMSO- or GW4869-treated neutrophils were incubated with anti-CD63 antibody-coated Dynabeads (Invitrogen) and detected using CD81-PE antibody in a bead-based flow cytometry assay. Inset: Inhibition was quantified using the relative median fluorescence intensity values from 3 independent experiments. **(B)** Representative tracks of chemotaxing differentiated PLB-985 cells under agarose towards a 50-pM/μm gradient of fMLP. Top left: NSshRNA cells stained with cytotracker red. Bottom left: SMPD2 sh1 cells stained with cytotracker red. Top right: NSshRNA cells stained with cytotracker green in a mixture of SMPD2 sh1 and NSshRNA cells. Bottom right: SMPD2 sh1 cells stained with cytotracker red in a mixture of SMPD2 sh1 and NSshRNA cells. The temporal location of cells in the X or Y direction is coded according to the colormap. Also see Fig 5A and 5B for further details. Raw data for panels A and B can be found in the Supporting Information section S2 Data file. fMLP, N-formylMethionyl-Leucyl-Phenylalanine; KD, knockdown; NSshRNA, nonspecific shRNA. (PDF)

S7 Fig. Paracrine action of exosomes on neutrophil chemotaxis. Representative tracks, speed, and CI of mixtures of cytotracker-labeled neutrophils treated with CsH, MK886, or GW4869 migrating under agarose towards an approximately 50 pM/μm gradient of fMLP. Speed and CI were calculated from the tracks of 40 cells and averaging over 4 independent movies. Raw data for panels A and B can be found in the Supporting information section S2 Data file. CI, chemotaxis index; CsH, cyclosporin H; fMLP, N-formylMethionyl-Leucyl-Phenylalanine.
(PDF)

S1 Movie. Localization of 5-LO in unstimulated mCherry-5LO cells. Differentiated cells expressing mCherry-5LO were plated on fibronectin-coated coverslips. Images were acquired every 30 s for 18 min. mCherry-5LO, mCherry-tagged 5-LO; 5-LO, 5-lipoxygenase.
(AVI)

S2 Movie. Localization of 5-LO in mCherry-5LO cells uniformly stimulated with fMLP. Differentiated PLB-985 cells expressing mCherry-5LO were plated on fibronectin-coated coverslips and uniformly stimulated with 10 nM fMLP. Images were acquired every 30 s for 5 min. fMLP, N-formylMethionyl-Leucyl-Phenylalanine; mCherry-5LO, mCherry-tagged 5-LO; 5-LO, 5-lipoxygenase.
(AVI)

S3 Movie. Redistribution of 5-LO in mCherry-5LO cells chemotaxing under agarose towards fMLP. Differentiated PLB-985 cells expressing mCherry-5LO were allowed to chemotax under agarose towards fMLP gradient on a coverslip coated with 0.2% gelatin. Time-lapse images were acquired every 30 s for 5 min, 700 μm away from the chemoattractant well. The movie represents a single Z-slice at 1.5 μm. Gradient slope approximately 50 pM/μm. fMLP, N-formylMethionyl-Leucyl-Phenylalanine; mCherry-5LO, mCherry-tagged 5-LO; 5-LO, 5-lipoxygenase.
(AVI)

S4 Movie. Co-localization of mCherry-5LO and CD63-GFP in cells chemotaxing under agarose towards fMLP. Differentiated PLB-985 cells were allowed to chemotax under agarose towards fMLP gradient on a coverslip coated with 0.2% gelatin. Time-lapse images were acquired every 10 s for 4 min, 700 μm away from the chemoattractant well. The movie represents a single Z-slice at 1.5 μm above coverslip. Gradient slope approximately 50 pM/μm. CD63-GFP, GFP-tagged CD63; fMLP, N-formylMethionyl-Leucyl-Phenylalanine; mCherry-5LO, mCherry-tagged 5-LO.
(AVI)

S5 Movie. Neutrophil chemotaxis towards fMLP, LTB$_4$, or exosomes. EZ-Taxiscan chemotaxis of neutrophils moving towards fMLP (10 nM), LTB$_4$ (100 nM), exosomes (100 μg/ml), or a buffer control. Images were acquired every 15 s for 60 min. fMLP, N-formylMethionyl-Leucyl-Phenylalanine; LTB$_4$, leukotriene B$_4$.
(MP4)

S6 Movie. Neutrophil chemotaxis towards LTB$_4$ or exosomes in the presence or absence of an LTB$_4$R1 antagonist. EZ-Taxiscan chemotaxis of neutrophils moving towards LTB$_4$ (100 nM) or exosomes (50 μg/ml). Cells were treated with either DMSO or the LTB$_4$R1 antagonist LY223982. Images were acquired every 15 s for 60 min. LTB$_4$, leukotriene B$_4$; LTB$_4$R1, receptor for LTB$_4$.
(MP4)

S7 Movie. Neutrophils chemotaxis towards exosomes purified from MK886-treated cells. EZ-Taxiscan chemotaxis of neutrophils chemotaxing towards 100 μg/ml exosomes purified from DMSO- or MK886-treated cells expressing mCherry-5LO. Images were acquired every 15 s for 50 min. mCherry-5LO, mCherry-tagged 5-LO.
(MP4)

S8 Movie. Chemotaxis of Rab27a and SMPD2 KD cells towards fMLP. EZ-Taxiscan chemotaxis of differentiated PLB-985 NSshRNA, Rab27ash1, Rab27ash3, SMPD2sh2, or SMPD2sh4 cells chemotaxing towards 1 nM fMLP. Images were acquired every 15 s for 30 min. fMLP, N-formylMethionyl-Leucyl-Phenylalanine; KD, knockdown; NSshRNA, nonspecific shRNA.
(MP4)

S9 Movie. Chemotaxis of Rab27a and SMPD2 KD cells towards fMLP. EZ-Taxiscan chemotaxis of differentiated PLB-985 NSshRNA, Rab27ash1, Rab27ash3, SMPD2sh2, and SMPD2sh4 cells moving towards 1 μM fMLP. Images were acquired every 15 s for 45 min. fMLP, N-formylMethionyl-Leucyl-Phenylalanine; KD, knockdown; NSshRNA, nonspecific shRNA.
(MP4)

S10 Movie. Chemotaxis of MK886-treated neutrophils in the presence of untreated neutrophils. DMSO-treated neutrophils stained with cytotracker red (left panel), MK886-treated neutrophils stained with cytotracker red (middle panel) and mixed populations of DMSO-treated neutrophils stained green and MK886-treated neutrophils stained red (right panel) were allowed to migrate under agarose towards fMLP gradient on a coverslip coated with 0.2% gelatin. Gradient slope approximately 50 pM/μm. Images were acquired every 60 s for 40 min. fMLP, N-formylMethionyl-Leucyl-Phenylalanine.
(MP4)

S11 Movie. Chemotaxis of GW4869-treated neutrophils in the presence of untreated neutrophils. DMSO-treated neutrophils stained with cytotracker red (left panel), GW4869-treated neutrophils stained with cytotracker red (middle panel) and mixed populations of DMSO-treated neutrophils stained green and GW4869-treated neutrophils stained red (right panel) were allowed to migrate under agarose towards fMLP gradient on a coverslip coated with 0.2% gelatin. Gradient slope approximately 50 pM/μm. Images were acquired every 60 s for 40 min. fMLP, N-formylMethionyl-Leucyl-Phenylalanine.
(MP4)

S12 Movie. Paracrine action of exosomes during neutrophil chemotaxis. Neutrophil stained with cytotracker green and treated with DMSO or CsH were mixed with inhibitor- or control-treated neutrophils stained with cytotracker red. The mixed cells were allowed to chemotax under agarose towards fMLP on a coverslip coated with 0.2% gelatin. Images were acquired every 60 s for 60 min. CsH, cyclosporin H; fMLP, N-formylMethionyl-Leucyl-Phenylalanine.
(MP4)

S1 Data. Raw data for all quantitative analyses in the main figures. Raw values for main Figs 1A and 1B, 2F and 2H, 3A and 3B, 4A–4D, 5A–5C, and 6A–6C are presented. The data are shown for each figure panel in a separate worksheet.
(XLSX)

S2 Data. Raw data for all quantitative analyses in the Supporting information figures. Raw values for S2A, S2B, S2D, S3A, S3B, S3C, S4C, S5A, S6A and S6B, S7A and S7B Figs are presented. The data are shown for each figure panel in a separate worksheet.
(XLSX)

S1 Raw images. Raw images for all western gels in the main and Supporting information figures. Raw images of western gels for Figs 1C, 2E and 2G, 3D and 3G, 4F, and S4A and S5B are presented.
(PDF)

Author Contributions

Conceptualization: Ritankar Majumdar, Carole A. Parent.

Data curation: Ritankar Majumdar, Carole A. Parent.

Formal analysis: Ritankar Majumdar, Subhash B. Arya, Carole A. Parent.

Funding acquisition: Carole A. Parent.

Investigation: Ritankar Majumdar, Aidin Tavakoli Tameh, Subhash B. Arya, Carole A. Parent.

Methodology: Ritankar Majumdar, Aidin Tavakoli Tameh, Subhash B. Arya, Carole A. Parent.

Project administration: Carole A. Parent.

Software: Ritankar Majumdar.

Supervision: Carole A. Parent.

Validation: Ritankar Majumdar, Aidin Tavakoli Tameh, Subhash B. Arya, Carole A. Parent.

Visualization: Ritankar Majumdar, Aidin Tavakoli Tameh, Subhash B. Arya, Carole A. Parent.

Writing – original draft: Ritankar Majumdar, Carole A. Parent.

Writing – review & editing: Ritankar Majumdar, Aidin Tavakoli Tameh, Subhash B. Arya, Carole A. Parent.

References

1. Majumdar R, Tavakoli Tameh A, Parent CA. Exosomes Mediate LTB4 Release during Neutrophil Chemotaxis. PLoS Biol. 2016; 14(1):e1002336. Epub 2016/01/08. https://doi.org/10.1371/journal.pbio.1002336 PMID: 26741884; PubMed Central PMCID: PMC4704783.

2. Jin T, Xu X, Hereld D. Chemotaxis, chemokine receptors and human disease. Cytokine. 2008; 44(1):1–8. https://doi.org/10.1016/j.cyto.2008.06.017 PMID: 18722135; PubMed Central PMCID: PMC2613022.

3. Kolaczkowska E, Kubes P. Neutrophil recruitment and function in health and inflammation. Nat Rev Immunol. 2013; 13(3):159–75. https://doi.org/10.1038/nri3399 PMID: 23435331

4. Majumdar R, Sixt M, Parent CA. New paradigms in the establishment and maintenance of gradients during directed cell migration. Curr Opin Cell Biol. 2014; 30(0):33–40. https://doi.org/10.1016/j.ceb.2014.05.010 PMID: 24959970; PubMed Central PMCID: PMC4177954.

5. Mahadeo DC, Parent CA. Signal relay during the life cycle of Dictyostelium. Curr Top Dev Biol. 2006; 73:115–40. https://doi.org/10.1016/S0070-2153(05)73004-0 PMID: 16782457.

6. Gouwy M, De Buck M, Portner N, Opdenakker G, Proost P, Struyf S, et al. Serum amyloid A chemoattracts immature dendritic cells and indirectly provokes monocyte chemotaxis by induction of cooperating CC and CXC chemokines. Eur J Immunol. 2015; 45(1):101–12. https://doi.org/10.1002/eji.201444818 PMID: 25345597.

7. Afonso PV, Janka-Junttila M, Lee YJ, McCann CP, Oliver CM, Aamer KA, et al. LTB4 is a signal-relay molecule during neutrophil chemotaxis. Dev Cell. 2012; 22(5):1079–91. https://doi.org/10.1016/j.devcel.2012.02.003 PMID: 22542839; PubMed Central PMCID: PMC4141281.

8. Needleman P, Turk J, Jakschik BA, Morrison AR, Lefkowith JB. Arachidonic acid metabolism. Annu Rev Biochem. 1986; 55:69–102. https://doi.org/10.1146/annurev.bi.55.070186.000441 PMID: 3017195.

9. Chou RC, Kim ND, Sadik CD, Seung E, Lan Y, Byrne MH, et al. Lipid-cytokine-chemokine cascade drives neutrophil recruitment in a murine model of inflammatory arthritis. Immunity. 2010; 33(2):266–78. https://doi.org/10.1016/j.immuni.2010.07.018 PMID: 20727790; PubMed Central PMCID: PMC3155777.

10. McDonald B, Kubes P. Chemokines: sirens of neutrophil recruitment-but is it just one song? Immunity. 2010; 33(2):148–9. https://doi.org/10.1016/j.immuni.2010.08.006 PMID: 20732637.

11. Oyoshi MK, He R, Li Y, Mondal S, Yoon J, Afshar R, et al. Leukotriene B4-driven neutrophil recruitment to the skin is essential for allergic skin inflammation. Immunity. 2012; 37(4):747–58. https://doi.org/10.1016/j.immuni.2012.06.018 PMID: 23063331; PubMed Central PMCID: PMC3478399.

12. Lammermann T, Afonso PV, Angermann BR, Wang JM, Kastenmuller W, Parent CA, et al. Neutrophil swarms require LTB4 and integrins at sites of cell death in vivo. Nature. 2013; 498(7454):371–5. https://doi.org/10.1038/nature12175 PMID: 23708969; PubMed Central PMCID: PMC3879961.

13. Uden AM, Hafstrom I, Palmblad J. Relation to chemotactic factor gradients to neutrophil migration and orientation under agarose. J Leukoc Biol. 1986; 39(1):27–35. https://doi.org/10.1002/jlb.39.1.27 PMID: 3001211.

14. Iwahashi M, Kasahara Y, Matsuzawa H, Yagi K, Nomura K, Terauchi H, et al. Self-diffusion, dynamical molecular conformation, and liquid structures of n-saturated and unsaturated fatty acids. J Phys Chem B. 2000; 104(26):6186–94. https://doi.org/10.1021/Jp000610l PubMed PMID: WOS:000088057100016.

15. Zsila F, Bikadi Z, Lockwood SF. In vitro binding of leukotriene B4 (LTB4) to human serum albumin: evidence from spectroscopic, molecular modeling, and competitive displacement studies. Bioorg Med Chem Lett. 2005; 15(16):3725–31. https://doi.org/10.1016/j.bmcl.2005.05.125 PMID: 15993588.

16. Greco V, Hannus M, Eaton S. Argosomes: a potential vehicle for the spread of morphogens through epithelia. Cell. 2001; 106(5):633–45. https://doi.org/10.1016/s0092-8674(01)00484-6 PMID: 11551510.

17. Entchev EV, Gonzalez-Gaitan MA. Morphogen gradient formation and vesicular trafficking. Traffic. 2002; 3(2):98–109. https://doi.org/10.1034/j.1600-0854.2002.030203.x PMID: 11929600.

18. Kriebel PW, Barr VA, Rericha EC, Zhang G, Parent CA. Collective cell migration requires vesicular trafficking for chemoattractant delivery at the trailing edge. J Cell Biol. 2008; 183(5):949–61. https://doi.org/10.1083/jcb.200808105 PMID: 19047467; PubMed Central PMCID: PMC2592838.

19. Faurschou M, Borregaard N. Neutrophil granules and secretory vesicles in inflammation. Microbes Infect. 2003; 5(14):1317–27. https://doi.org/10.1016/j.micinf.2003.09.008 PMID: 14613775.

20. Kobayashi T, Vischer UM, Rosnoblet C, Lebrand C, Lindsay M, Parton RG, et al. The tetraspanin CD63/lamp3 cycles between endocytic and secretory compartments in human endothelial cells. Mol Biol Cell. 2000; 11(5):1829–43. https://doi.org/10.1091/mbc.11.5.1829 PMID: 10793155; PubMed Central PMCID: PMC14887.

21. Cieutat AM, Lobel P, August JT, Kjeldsen L, Sengelov H, Borregaard N, et al. Azurophilic granules of human neutrophilic leukocytes are deficient in lysosome-associated membrane proteins but retain the mannose 6-phosphate recognition marker. Blood. 1998; 91(3):1044–58. PMID: 9446668.

22. Tucker KA, Lilly MB, Heck L Jr., Rado TA. Characterization of a new human diploid myeloid leukemia cell line (PLB-985) with granulocytic and monocytic differentiating capacity. Blood. 1987; 70(2):372–8. PMID: 3475136.

23. Raposo G, Stoorvogel W. Extracellular vesicles: exosomes, microvesicles, and friends. J Cell Biol. 2013; 200(4):373–83. https://doi.org/10.1083/jcb.201211138 PMID: 23420871; PubMed Central PMCID: PMC3575529.

24. Andreu Z, Yanez-Mo M. Tetraspanins in extracellular vesicle formation and function. Front Immunol. 2014; 5:442. https://doi.org/10.3389/fimmu.2014.00442 PMID: 25278937; PubMed Central PMCID: PMC4165315.

25. Hess C, Sadallah S, Hefti A, Landmann R, Schifferli JA. Ectosomes released by human neutrophils are specialized functional units. J Immunol. 1999; 163(8):4564–73. PMID: 10510400.

26. Lancaster GI, Febbraio MA. Exosome-dependent trafficking of HSP70: a novel secretory pathway for cellular stress proteins. J Biol Chem. 2005; 280(24):23349–55. https://doi.org/10.1074/jbc.M502017200 PMID: 15826944.

27. Ostrowski M, Carmo NB, Krumeich S, Fanget I, Raposo G, Savina A, et al. Rab27a and Rab27b control different steps of the exosome secretion pathway. Nat Cell Biol. 2010; 12(1):19–30; sup pp 1–13. https://doi.org/10.1038/ncb2000 PMID: 19966785.

28. Bobrie A, Krumeich S, Reyal F, Recchi C, Moita LF, Seabra MC, et al. Rab27a supports exosome-dependent and -independent mechanisms that modify the tumor microenvironment and can promote tumor progression. Cancer Res. 2012; 72(19):4920–30. https://doi.org/10.1158/0008-5472.CAN-12-0925 PMID: 22865453.

29. Trajkovic K, Hsu C, Chiantia S, Rajendran L, Wenzel D, Wieland F, et al. Ceramide triggers budding of exosome vesicles into multivesicular endosomes. Science. 2008; 319(5867):1244–7. https://doi.org/10.1126/science.1153124 PMID: 18309083.

30. Stenfeldt A-L, Karlsson J, Wennerås C, Bylund J, Fu H, Dahlgren C. Cyclosporin H. Boc-MLF and Boc-FLFLF are Antagonists that Preferentially Inhibit Activity Triggered Through the Formyl Peptide Receptor. Inflammation. 2007; 30(6):224–9. https://doi.org/10.1007/s10753-007-9040-4 PMID: 17687636

31. Esser J, Gehrmann U, D'Alexandri FL, Hidalgo-Estevez AM, Wheelock CE, Scheynius A, et al. Exosomes from human macrophages and dendritic cells contain enzymes for leukotriene biosynthesis and promote granulocyte migration. J Allergy Clin Immunol. 2010; 126(5):1032–40, 40 e1-4. https://doi.org/10.1016/j.jaci.2010.06.039 PMID: 20728205.

32. Schorey JS, Cheng Y, Singh PP, Smith VL. Exosomes and other extracellular vesicles in host-pathogen interactions. EMBO Rep. 2015; 16(1):24–43. https://doi.org/10.15252/embr.201439363 PMID: 25488940; PubMed Central PMCID: PMC4304727.

33. Gasser O, Schifferli JA. Activated polymorphonuclear neutrophils disseminate anti-inflammatory microparticles by ectocytosis. Blood. 2004; 104(8):2543–8. https://doi.org/10.1182/blood-2004-01-0361 PMID: 15213101.

34. Sadallah S, Eken C, Schifferli JA. Ectosomes as modulators of inflammation and immunity. Clin Exp Immunol. 2011; 163(1):26–32. https://doi.org/10.1111/j.1365-2249.2010.04271.x PMID: 21039423; PubMed Central PMCID: PMC3010909.

35. Singh RK, Liao W, Tracey-White D, Recchi C, Tolmachova T, Rankin SM, et al. Rab27a-mediated protease release regulates neutrophil recruitment by allowing uropod detachment. J Cell Sci. 2012; 125(Pt 7):1652–6. https://doi.org/10.1242/jcs.100438 PMID: 22375060; PubMed Central PMCID: PMC3346826.

36. Colvin RA, Means TK, Diefenbach TJ, Moita LF, Friday RP, Sever S, et al. Synaptotagmin-mediated vesicle fusion regulates cell migration. Nat Immunol. 2010; 11(6):495–502. https://doi.org/10.1038/ni.1878 PMID: 20473299; PubMed Central PMCID: PMC2951881.

37. Sung BH, Ketova T, Hoshino D, Zijlstra A, Weaver AM. Directional cell movement through tissues is controlled by exosome secretion. Nat Commun. 2015; 6:7164. https://doi.org/10.1038/ncomms8164 PMID: 25968605; PubMed Central PMCID: PMC4435734.

38. Subra C, Grand D, Laulagnier K, Stella A, Lambeau G, Paillasse M, et al. Exosomes account for vesicle-mediated transcellular transport of activatable phospholipases and prostaglandins. J Lipid Res. 2010; 51(8):2105–20. https://doi.org/10.1194/jlr.M003657 PMID: 20424270; PubMed Central PMCID: PMC2903822.

39. Christianson HC, Svensson KJ, van Kuppevelt TH, Li JP, Belting M. Cancer cell exosomes depend on cell-surface heparan sulfate proteoglycans for their internalization and functional activity. Proc Natl Acad Sci U S A. 2013; 110(43):17380–5. https://doi.org/10.1073/pnas.1304266110 PMID: 24101524; PubMed Central PMCID: PMC3808637.

40. Rius M, Hummel-Eisenbeiss J, Keppler D. ATP-dependent transport of leukotrienes B4 and C4 by the multidrug resistance protein ABCC4 (MRP4). J Pharmacol Exp Ther. 2008; 324(1):86–94. https://doi.org/10.1124/jpet.107.131342 PMID: 17959747.

41. Sitrin RG, Sassanella TM, Petty HR. An obligate role for membrane-associated neutral sphingomyelinase activity in orienting chemotactic migration of human neutrophils. Am J Respir Cell Mol Biol. 2011; 44(2):205–12. https://doi.org/10.1165/rcmb.2010-0019OC PMID: 20378749; PubMed Central PMCID: PMC3049232.

42. Simons M, Raposo G. Exosomes–vesicular carriers for intercellular communication. Curr Opin Cell Biol. 2009; 21(4):575–81. https://doi.org/10.1016/j.ceb.2009.03.007 PMID: 19442504

43. Sadik CD, Luster AD. Lipid-cytokine-chemokine cascades orchestrate leukocyte recruitment in inflammation. J Leukoc Biol. 2012; 91(2):207–15. https://doi.org/10.1189/jlb.0811402 PMID: 22058421; PubMed Central PMCID: PMC3290425.

44. Satpathy SR, Jala VR, Bodduluri SR, Krishnan E, Hegde B, Hoyle GW, et al. Crystalline silica-induced leukotriene B4-dependent inflammation promotes lung tumour growth. Nat Commun. 2015; 6:7064. https://doi.org/10.1038/ncomms8064 PMID: 25923988; PubMed Central PMCID: PMC4418220.

45. Mahadeo DC, Janka-Junttila M, Smoot RL, Roselova P, Parent CA. A chemoattractant-mediated Gi-coupled pathway activates adenylyl cyclase in human neutrophils. Mol Biol Cell. 2007; 18(2):512–22. https://doi.org/10.1091/mbc.e06-05-0418 PMID: 17135293; PubMed Central PMCID: PMC1783842.

46. Liu L, Das S, Losert W, Parent CA. mTORC2 regulates neutrophil chemotaxis in a cAMP- and RhoA-dependent fashion. Dev Cell. 2010; 19(6):845–57. https://doi.org/10.1016/j.devcel.2010.11.004 PMID: 21145500; PubMed Central PMCID: PMC3071587.

47. Tauro BJ, Greening DW, Mathias RA, Ji H, Mathivanan S, Scott AM, et al. Comparison of ultracentrifugation, density gradient separation, and immunoaffinity capture methods for isolating human colon cancer cell line LIM1863-derived exosomes. Methods. 2012; 56(2):293–304. https://doi.org/10.1016/j.ymeth.2012.01.002 PMID: 22285593.

48. Comer FI, Parent CA. Phosphoinositide 3-kinase activity controls the chemoattractant-mediated activation and adaptation of adenylyl cyclase. Mol Biol Cell. 2006; 17(1):357–66. https://doi.org/10.1091/mbc.e05-08-0781 PMID: 16267269; PubMed Central PMCID: PMC1345673.

49. Ohi M, Li Y, Cheng Y, Walz T. Negative Staining and Image Classification—Powerful Tools in Modern Electron Microscopy. Biol Proced Online. 2004; 6:23–34. Epub 2004/04/23. https://doi.org/10.1251/bpo70 PMID: 15103397; PubMed Central PMCID: PMC389902.

50. Schneider CA, Rasband WS, Eliceiri KW. NIH Image to ImageJ: 25 years of image analysis. Nat Methods. 2012; 9(7):671–5. Epub 2012/08/30. https://doi.org/10.1038/nmeth.2089 PMID: 22930834; PubMed Central PMCID: PMC5554542.

51. McCann CP, Kriebel PW, Parent CA, Losert W. Cell speed, persistence and information transmission during signal relay and collective migration. J Cell Sci. 2010; 123(Pt 10):1724–31. https://doi.org/10.1242/jcs.060137 PMID: 20427323; PubMed Central PMCID: PMC2864714.

52. McColl SR, Betts WH, Murphy GA, Cleland LG. Determination of 5-lipoxygenase activity in human polymorphonuclear leukocytes using high-performance liquid chromatography. J Chromatogr. 1986; 378 (2):444–9. https://doi.org/10.1016/s0378-4347(00)80740-9 PMID: 3016012